NASA Contractor Report 190798

Digital Active Material Processing Platform Effort (Damper), SBIR Phase II

John Blackburn and Dennis Smith
Applied Technology Associates
Albuquerque, NM

November 1992

INTRODUCTION

Applied Technology Associates, Inc., (ATA) has demonstrated that inertial actuation can be employed effectively in digital, active vibration isolation systems. Inertial actuation involves the use of momentum exchange to produce corrective forces which act directly on the payload being actively isolated. In a typical active vibration isolation system, accelerometers are used to measure the inertial motion of the payload. The signals from the accelerometers are then used to calculate the corrective forces required to counteract, or "cancel out" the payload motion. Active vibration isolation is common technology, but the use of inertial actuation in such systems is novel, and is the focus of the DAMPER project.

In May of 1991 a report was completed which documented the successful demonstration of inertial actuation, employed in the control of vibration in a single axis[1]. In the one-degree-of-freedom (1DOF) experiment a set of air bearing rails was used to suspend the payload, simulating a microgravity environment in a single horizontal axis. Digital Signal Processor (DSP) technology was used to calculate in real time, the control law between the accelerometer signals and the inertial actuators. The data obtained from this experiment verified that as much as 20 dB of rejection could be realized by this type of system.

Included in this report is a discussion of recent tests performed by ATA in which vibrations were actively controlled in three axes simultaneously. In the three-degree-of-freedom (3DOF) system, the air bearings were designed in such a way that the payload is free to rotate about the azimuth axis, as well as translate in the two horizontal directions.

This is the final report on the DAMPER project. It is a culmination of past (1DOF) and present (3DOF) work, and is intended to provide an overall picture of the project. The actuator developed for the DAMPER project has applications beyond payload isolation, including structural damping and source vibration isolation. This report includes a brief discussion of these applications, as well as a commercialization plan for the actuator.

---

[1]. Reference is made here to the ATA report entitled "Digital Active Materials Processing Experiment (DAMPER) 1DOF Platform Development Task Final Report".

1.0 PROGRAM OBJECTIVES

1.1 Scope

The first objective of the DAMPER project was to develop a linear, inertial actuator suitable for space stabilization applications. An inertial actuator operates on the principle of momentum interchange. The key component of this type of actuator is an inertial mass, which is caused to accelerate by imposing on it a force (usually applied by magnetic fields). When the inertial mass accelerates, it produces an equal and opposite force on the actuator housing. The actuator housing in turn transmits that force to the surface to which the actuator is mounted. Inertial actuation differs fundamentally from traditional forms of actuation because there is no mechanical connection between a fixed point and the surface to be actuated. In contrast, an electromagnetic (or so-called "voice coil") actuator is used to apply forces between two surfaces. This is an example of a relative force actuator.

The inertial actuator had to meet certain requirements. The requirements of the actuator involved the frequency response, the throw, the force constant, and the peak force. The peak force can be increased at the expense of the frequency response, and vice versa, so there were tradeoffs involved in the design. The actuator requirements were based on measurements of the disturbance environment, as well as the desired bandwidth of the vibration isolation.

The second objective of the DAMPER program was to demonstrate the use of inertial actuators in one and three-axis, active isolation systems. Once the actuators were designed and fabricated, vibration isolation systems were developed to demonstrate their performance. It should be noted however, that the development and performance of the overall isolation systems was *not* the focus of the project. There are factors other than the performance of the actuators which limit the overall performance of vibration isolation systems. These factors include sensor noise and dynamics, the dynamic coupling between the axes of controlled motion and the speed of the digital computer, to name a few. There are data sets presented in this report which suggest that the isolation systems used to test the actuators may not provide the levels of disturbance rejection required for many micro-g science applications. In these cases it is shown that the actuators are not the limiting factor.

As an aside, a distinction is made in active vibration isolation technology between source and payload isolation. When vibrations originate from the payload, and the objective is to reduce the levels of vibration which reach the environment, then a *source* vibration isolation system is

required. A system which is intended to abate vibration disturbances which act on the payload is called a *payload* vibration isolation system. At the time this work was solicited, the micro-g science community was especially interested in the payload isolation problem. For this reason payload isolation schemes were selected to demonstrate the performance of the actuators, and the performance of the isolation systems was assessed according to payload isolation specifications.

Theoretically, there should be no difference between the disturbance rejection that can be realized by a payload isolation system employing inertial actuators, and a similar system employing one of the more common actuator designs (such as "voice coil" actuators for example). The second objective of the DAMPER project involved obtaining test data which supports this theory. The data does imply that inertial and relative force actuators are equivalent in payload isolation schemes. However, hindsight suggests that implementation of the actuators in a source vibration system may have proven to be a more dramatic demonstration of the merits of inertial actuation. Inertial actuation is clearly superior to relative force actuation in the solution of source vibration and structural damping problems. More will be said about these applications later.

1.2 Actuator Development

The primary objective of the actuator development was to demonstrate that the inertial actuation concept could be implemented in hardware, and customized to meet specific design goals. The design of the actuator had to address the key issues listed below.

1) The force constant and peak force;
2) The frequency response;
3) The throw;
4) Stiction between the moving actuator coil and the inner conductor;
5) Low frequency caging of the moving actuator coil position;
6) Electronic noise.

Each of these issues is discussed in the next section. It should be noted however, that the actuator design discussed in the next section is based on the specific payload isolation problem selected to demonstrate the performance. The design would have to be modified to meet significantly different requirements.

1.3 Vibration Isolation System Development

The inertial actuator was designed for vibration isolation applications, and thus it was necessary to demonstrate the performance of the actuator in actual isolation systems. The second objective of the DAMPER project was to develop and test two isolation systems, both employing the actuators. The first system was intended to demonstrate active payload isolation in a single axis, and the second was designed to demonstrate that the actuators can be used to control vibration in three axes simultaneously. The two systems will hereafter be referred to as the 1DOF and the 3DOF systems, respectively.

The desired performance of the isolation systems was based on specifications provided by the International Astronautical Federation (IAF). In Figure 1-1 envelopes which specify the maximum allowable vibration levels for various processes, are presented as a function of frequency. ATA derived from this set of curves (provided by the IAF), a single envelope under which residual vibration should fall. This envelope is shown in Figure 1-2.

The envelope shown in Figure 1-2 limits only vibrations in the frequency band from 0.1 to 100 Hz. In order to accomplish vibration isolation at frequencies significantly below 0.1 Hz, the throw of an inertial actuator would have to be relatively large (as much as 2 feet). Large-throw actuators could indeed be designed to accommodate very low frequency isolation. However, the demonstration of vibration isolation at 0.1 Hz is sufficient to show the validity of the approaches used.

In order to realize optimal performance from a vibration isolation system, the bandwidth of the control system should be as high as possible. The bandwidth of the control system dictates the highest frequency at which disturbance rejection can be realized by the system. In general the bandwidth is limited by the phase margin. Phase loss due to sensor dynamics and sampling cause the phase margin to deteriorate at frequencies above 100 Hz. Since it was known at the outset that active isolation above 100 Hz would not be possible with the available sensors and computer, the performance specifications were defined from 0.1 to 100 Hz. The envelope shown in Figure 1-2 corresponds to the most conservative curves in Figure 1-1, within the frequency band 0.1 to 100 Hz.

1.4 Commercialization

The third and final goal of the project was to formulate a plan to market the inertial actuator as a commercial product. As mentioned earlier, these actuators have applications in both source and payload vibration isolation, as well as in the active damping of large space structures.

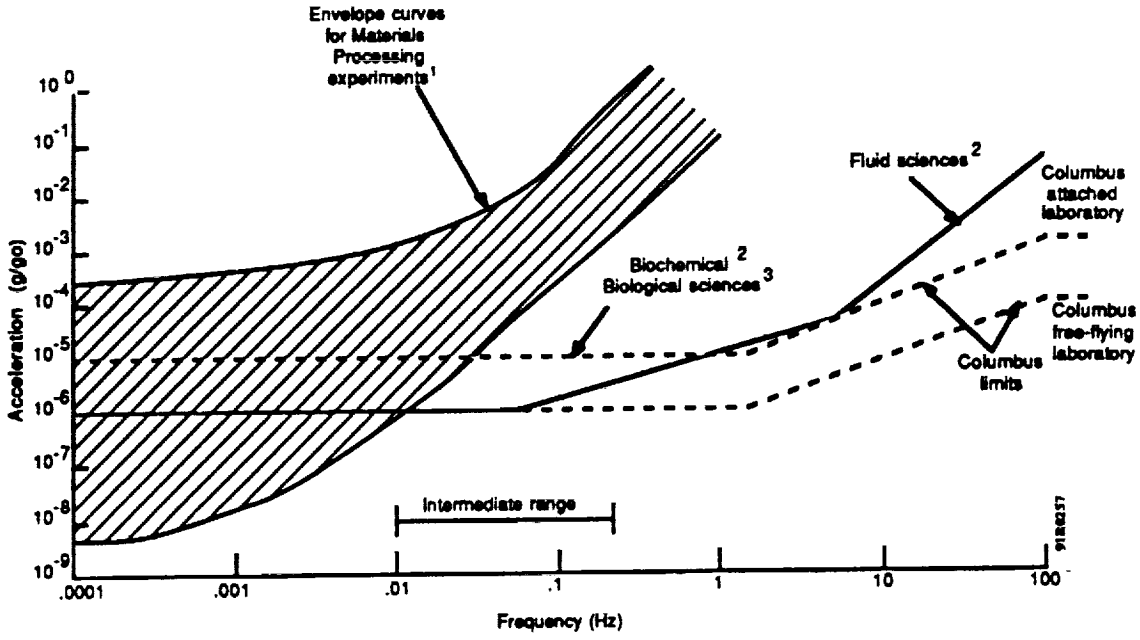

Figure 1-1. Acceleration Sensitivity of Microgravity Experiments

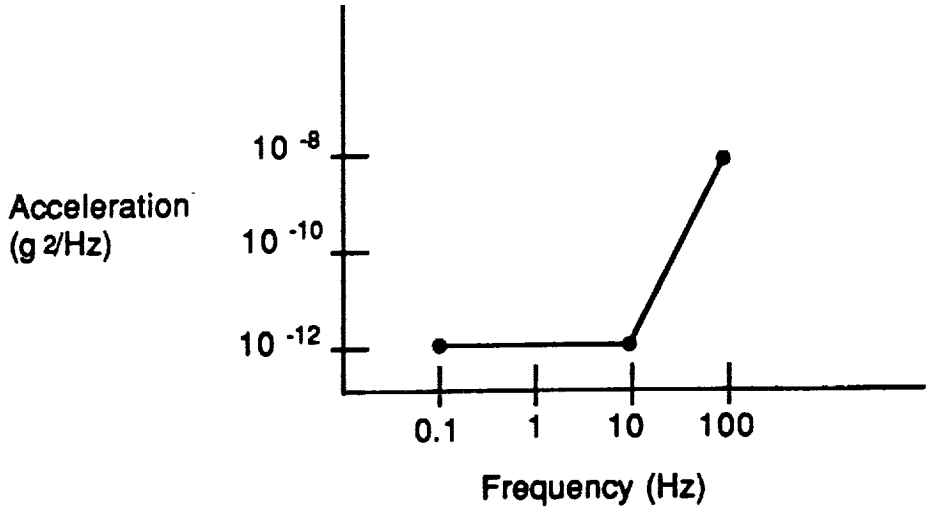

Figure 1-2. Residual Platform Acceleration Profile

2.0 DESIGNING THE ACTUATOR

2.1 Principle of Operation

Figure 2-1 is a schematic of an electromagnetic, linear, inertial actuator[2]. Permanent magnets are attached to the actuator housing such that they surround the moving actuator coil and the inner conductor. The moving actuator coil is a spool of copper wire which is wound so that the wire turns encircle the inner conductor. The moving actuator coil is free to slide along the axis of the inner conductor.

When a current is passed through the wire turns of the moving actuator coil, a force is created which has a magnitude that is proportional to the magnitude of the cross product of the current vector $\underline{\mathbf{i}}$, and the magnetic field vector $\underline{\mathbf{B}}$. The current flows in the circumferential direction, and the magnetic field flux lines created by the permanent magnets are directed radially toward the center of, and normal to the axis of the inner conductor. Thus, the vector cross product of $\underline{\mathbf{i}}$ and $\underline{\mathbf{B}}$ yields a force vector $\underline{\mathbf{F}}$, which is directed along the axis of the inner conductor.

$$F_m = \propto |\underline{\mathbf{i}} \times \underline{\mathbf{B}}| \qquad (1)$$

where:

$\propto = 2\pi r_{mean} N$

r_{mean} = mean spool radius (cm)

N = number of coil windings

Assuming that the vectors $\underline{\mathbf{i}}$ and $\underline{\mathbf{B}}$ are always normal to each other, the magnitudes of these vectors can be denoted as i and B respectively, and equation (1) can be written as

$$F_m = 2\pi r_{mean} NBi \qquad (2)$$

---

2. The actuator shown in Figure 2.1 does not have exactly the configuration of the ones used in the final DAMPER isolation systems. It is quite similar however, and the schematic provides a good illustration of the principle of operation.

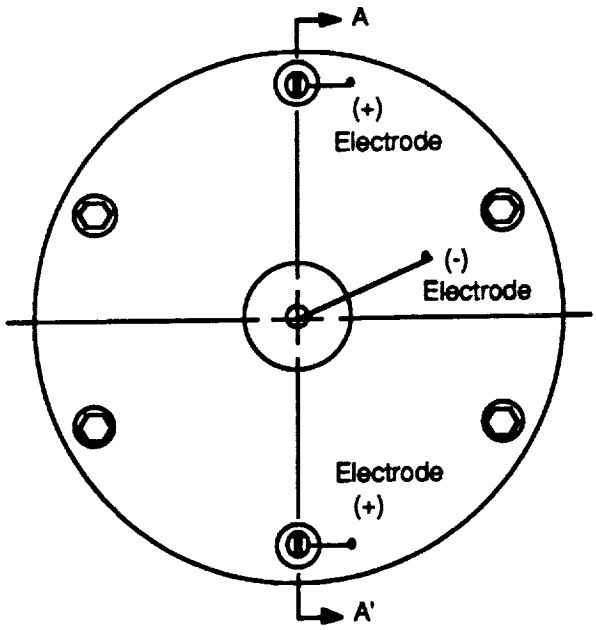

Size: Length ~ 60 cm (24 in), 5cm (2 in) Diameter
Weight: 10 kg (22 lbs)

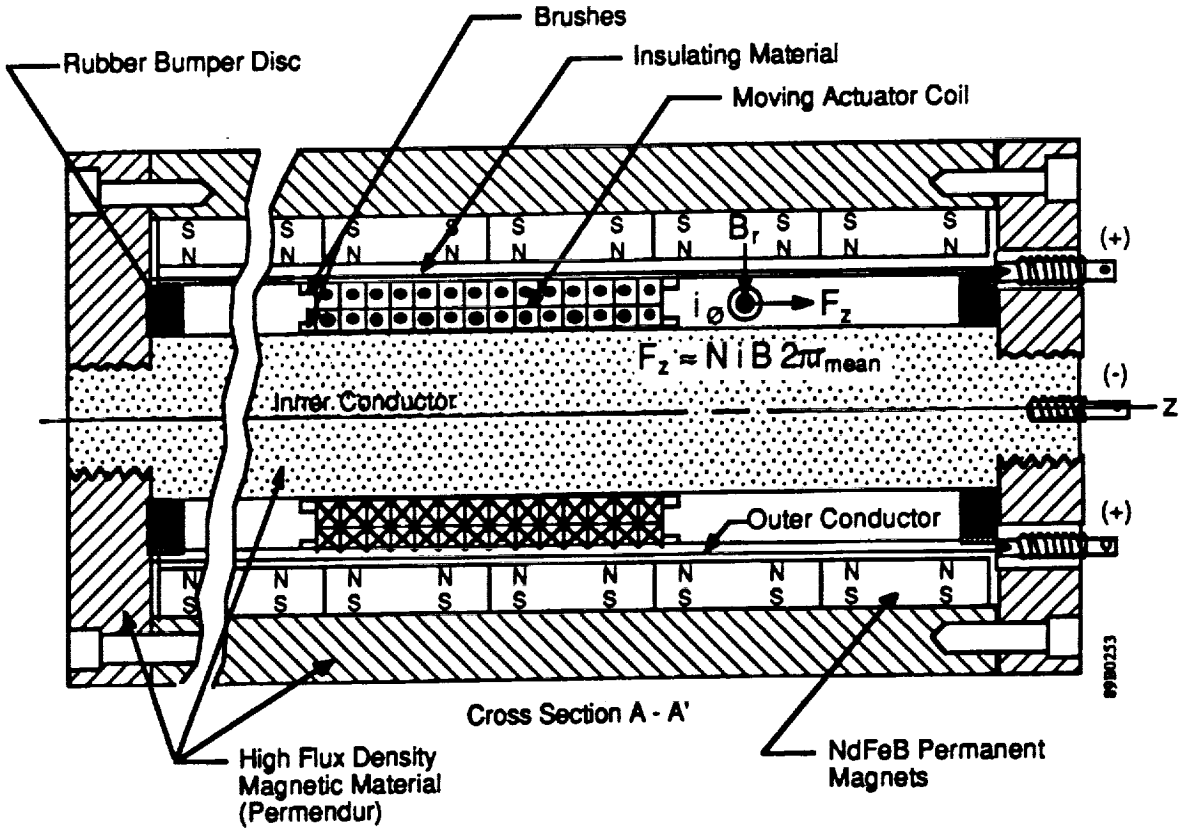

Figure 2-1. Principle of Operation of Electromagnetic, Linear, Inertial Actuator

Defining the motor constant K_m as follows:

$$K_m = 2\pi r_{mean} NB \tag{3}$$

The electromagnetic force can be written as follows:

$$F_m = K_m i \tag{4}$$

Note that a change in the polarity of the current (or voltage) will reverse the sign, and thus the direction of the force F_z.

When the force F_m acts on the moving actuator coil, an equal and opposite force acts on the housing of the actuator. This force is then transmitted to the surface to which the actuator is mounted, forcing that surface to accelerate.

2.2 Magnetic Flux Line Considerations

The operation of the actuator depends on closed magnetic circuit paths which encircle air gaps between the permanent magnet assemblies and the inner conductor. A typical family of magnetic flux paths is shown in Figure 2-2.

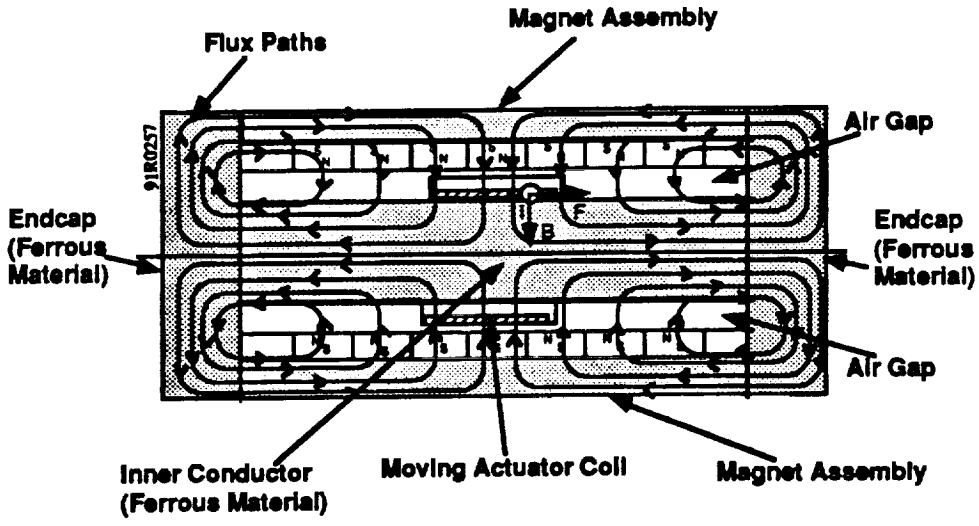

Figure 2-2. Magnetic Flux Lines in Inertial Actuator

Notice that the direction of the resulting magnetic force **F**, is along the axis of the inner conductor. Notice also that the ferrous end caps are a crucial component of the magnetic circuit. The ferrous material of which the magnetic circuit components (magnet assemblies, end caps and inner conductor) are composed is Venadium Permendur, which has a high magnetic saturation flux density.

2.3 Frequency Response

2.3.1 Specifying the Mass of the Moving Actuator Coil

From a dynamic standpoint, the performance of a linear inertial actuator improves as the mass of the moving actuator coil is increased. The reason is that larger coil masses can induce larger inertial forces on the payload. The effect of increasing the moving actuator coil mass can be observed in the frequency domain.

Consider the single-degree-of-freedom system shown in Figure 2-3. The mass m_1 represents the combined mass of the isolated payload and actuator housing. The inertial mass m_1 is free to translate with respect to ground without resistance, and is acted upon by a disturbance force F_d. The mass m_2 represents the moving actuator coil which is free to translate with respect to the mass m_1. Relative motion of the masses m_1 and m_2 is caused by the electromagnetic force F_m.

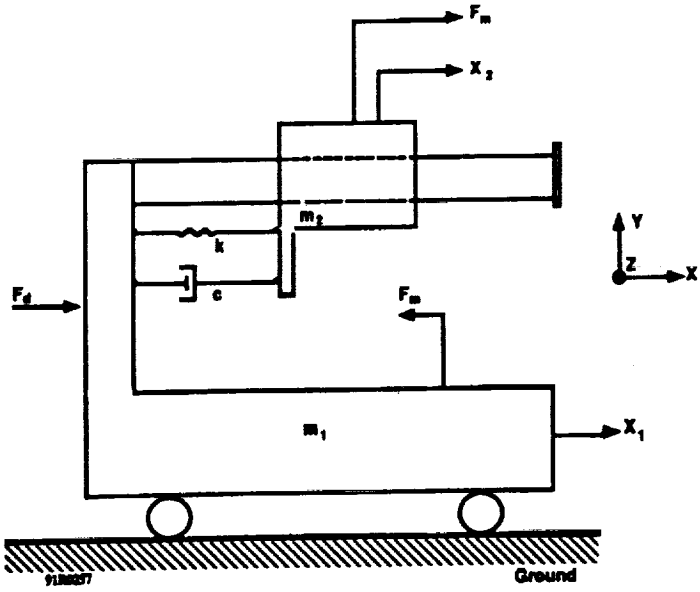

Figure 2-3. Combined Inertial Actuator/1DOF Platform System

It is necessary in the design of real-world actuators to "cage" the position of the moving actuator coil, so that it is operates roughly in the center of the inner conductor. Without a caging mechanism of some kind in place, the moving actuator coil collides with the end caps during operation. Such collisions impose disturbances on the payload. This is undesirable since the ultimate goal of an isolation system employing the actuator is to remove disturbances. In reality the caging is done electronically. However, it is convenient (and reasonable) to approximate the dynamics of the caging circuit by a mechanical spring k (see Figure 2-3).

There is a certain amount of sliding friction which takes place between the moving actuator coil and the inner conductor. This sliding, or *coulombic* friction is actually a non-linear function, but it can be approximated by a linear dashpot having a damping coefficient, c (see Figure 2-3).

The system in Figure 2-3 is broken down into two free-body diagrams which are presented in Figure 2-4. All the forces acting on the two masses are depicted in the diagrams. Using Newton's second law, the equations of motion for each mass can be derived from the free-body diagrams.

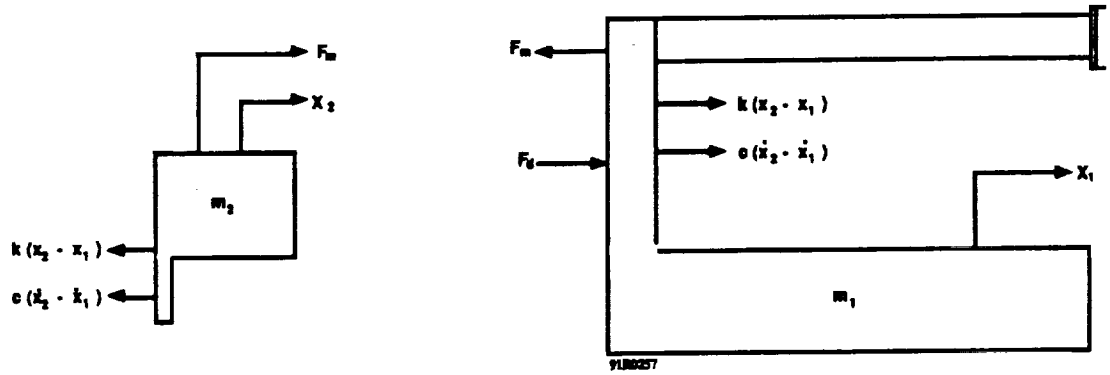

Figure 2-4. Free-Body Diagrams of Masses m_1 and m_2

$$\Sigma F_1 = m_1 \frac{d^2x_1}{dt^2} = c\left(\frac{dx_2}{dt} - \frac{dx_1}{dt}\right) + k(x_2 - x_1) - F_m + F_d \qquad (5)$$

$$\Sigma F_2 = m_2 \frac{d^2x_2}{dt^2} = -c\left(\frac{dx_2}{dt} - \frac{dx_1}{dt}\right) - k(x_2 - x_1) + F_m \qquad (6)$$

The Laplace transforms of equations (5) and (6) follows:

$$X_1(s)[s^2 + (c/m_1)s + (k/m_1)] - X_2(s)[(c/m_1)s + (k/m_1)]$$

$$= - F_m(s) + F_d(s) \tag{7}$$

$$X_2(s)[s^2 + (c/m_2)s + (k/m_2)] - X_1(s)[(c/m_2)s + (k/m_2)]$$

$$= F_m(s) \tag{8}$$

The Laplace transform of equation (4) is also required.

$$F_m(s) = K_m I(s) \tag{9}$$

Equations (7), (8) and (9) are then combined to obtain the ratio $(s^2X_1(s))/I(s)$. This ratio is the transfer function from the actuator current input to the acceleration of the payload. The magnitude Bode plots of this transfer function are shown for various N, in Figure 2-5. Note that the mass m_2 is related to the number of turns N.

$$m_2 = m_0 + \beta N \tag{10}$$

where: m_0 = weight of the bobbin (gms)

β = mass of wire per turn (gms/turn)

The amount of force which must be provided by the actuator is of course, dependent upon the application. For payload vibration isolation systems, the required force is specified by the nature of the disturbances acting on the payload. The power spectral density function associated with the uncontrolled vibration environment on the payload is integrated to obtain the cumulative power, or "cum-power". The cum-power is a single number having the units g^2. The square root of this value is the root-mean-square (rms) of the vibration disturbance to be abated (units of g). The peak force required of the actuator is then the product of the rms acceleration and the mass of the payload (including the actuators). It is advisable to provide more force than the above calculations dictate, in order to insure that whatever impulsive forces acting on the payload can be abated as well.

Figure 2-6 is the power spectral density of the vibration disturbances measured on the payload of the 1DOF experiment, while the payload was supported with an air bearing. The rms of this

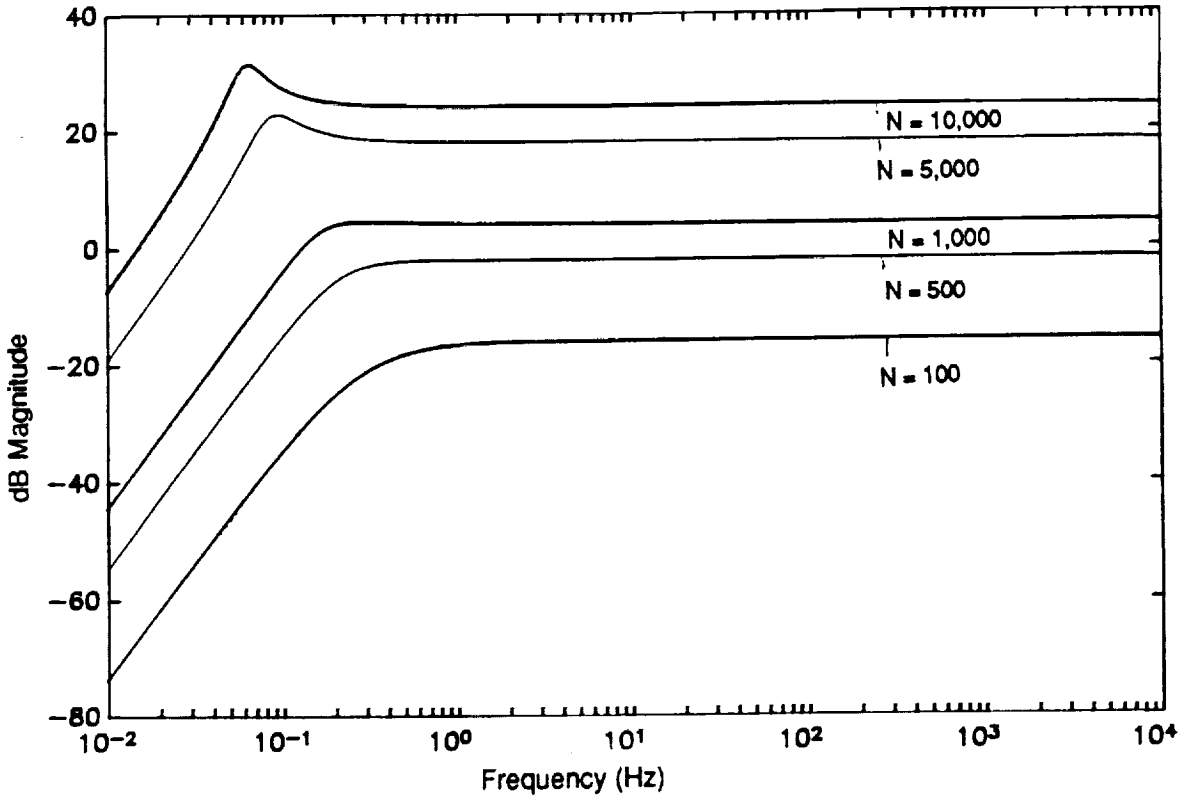

Figure 2-5. Magnitude Bode Plots of the Ratio $s^2X_1(s)/I(s)$ for Various N

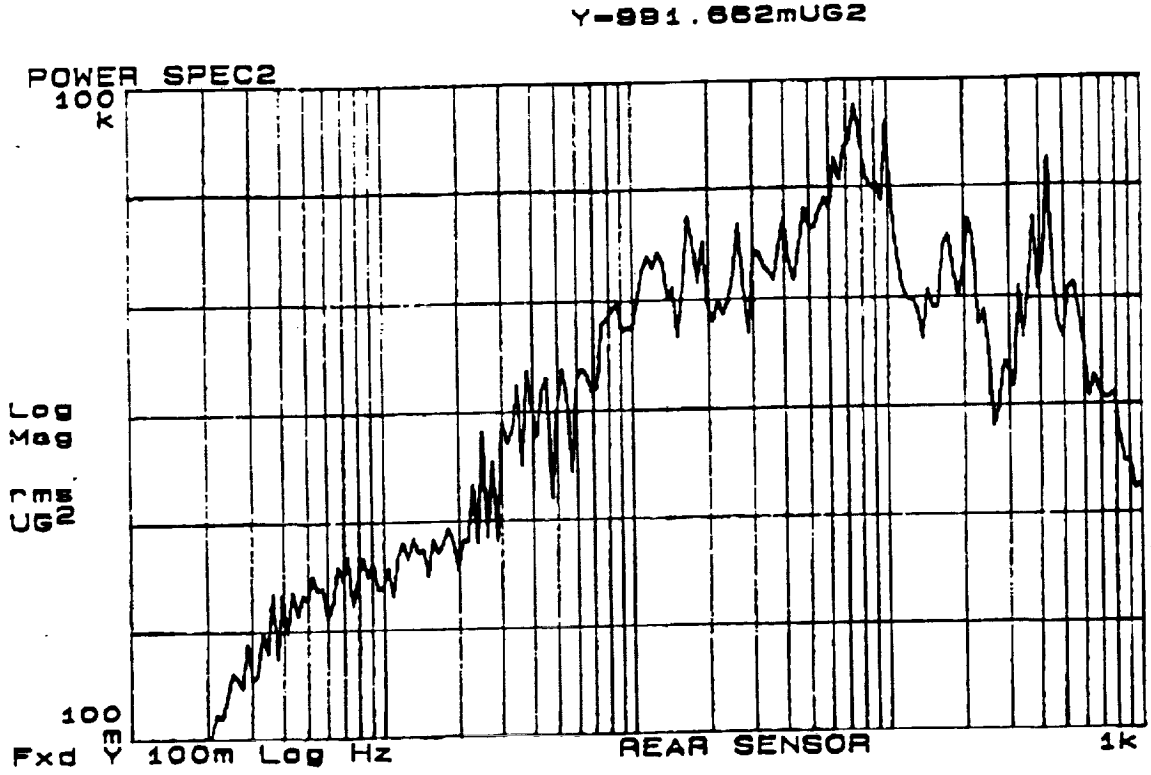

Figure 2-6. Disturbance PSD Measured on Carriage With No Control

function is about 2 milli-g, depending on the time of day the psd is obtained. For a 50-pound payload the force required to abate a 2-milli-g disturbance is about 0.5 Newtons. A value of 2.0 Newtons was chosen, allowing a factor of safety of 4.

2.3.2 Inductance Considerations

The moving actuator coil is in itself an AC circuit. A simple circuit diagram of the coil is shown in Figure 2-7. In this figure R_a and L_a are the resistance and inductance of the windings, respectively. The current flowing through the circuit is denoted i_a.

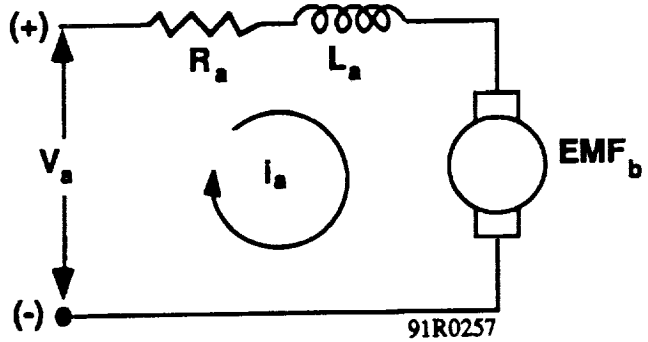

Figure 2-7. Circuit Diagram for Armeture (Moving Coil)

An opposing voltage, or "back-emf" is created which is proportional to the relative velocity between the masses m_1 and m_2 as shown below.

$$EMF_b = K_g \left(\frac{dx_2}{dt} - \frac{dx_1}{dt} \right) \tag{11}$$

where: K_g = generator constant (kg*m/A*s)

The differential equation which describes the voltage and current behavior of the circuit, is obtained by Kirchoff's Voltage Law. The sum of all the voltages around a closed path is equal to zero.

$$-v_a + i_a R_a + L_a \frac{di_a}{dt} + K_g \left(\frac{dx_2}{dt} - \frac{dx_1}{dt} \right) = 0 \tag{12}$$

The Laplace transform of this equation is presented below.

$$V_a(s) = I_a(s)(L_a s + R_a) + X_2(s)K_g s - X_1(s)K_g s \tag{13}$$

By combining equations (7), (8), (9) and (13) the ratio of $V_a(s)$ to $I_a(s)$ can be obtained. Bode plots of this transfer function are shown in Figure 2-8.

Notice that the magnitude function of the response shown in Figure 2-8 rises at 20 dB/decade above about 8 Hz. This behavior is typical of an inductive circuit. As the inductance is increased, the frequency at which the magnitude function begins to rise, decreases. Another way to express the same ideas is that the amount of voltage required to drive the coil increases with frequency, and with increasing inductance. The inductance L_a is related to the number of coil turns N, by the relation below.

$$L_a = N^2/R_e \tag{14}$$

where: R_e = reluctance ($A^2*s^2/kg*m^2$)

The reluctance is to a magnetic circuit, what resistance is to an electric circuit.

Based on the above arguments, there is a tradeoff between the mass and the inductance of the moving actuator coil. Increasing the moving actuator coil mass improves the actuator from a dynamic standpoint. However, the larger number of coil turns associated with the increased mass, requires more voltage from the drive electronics.

The Bode plots in Figure 2-5 depict the acceleration response of the actuator/payload system to a current input. Above the frequency corner of the coil position caging loop[3], this function is a constant. This function is much easier to work with than the response to voltage commands. Figure 2-9 shows the acceleration response of the actuator/payload system to a voltage input.

A current amplifier is employed in the actuator circuitry to provide current outputs which are directly proportional to voltage inputs.

3. Recall that an electronic spring is used to insure that the moving actuator coil remains roughly in the center of the inner conductor.

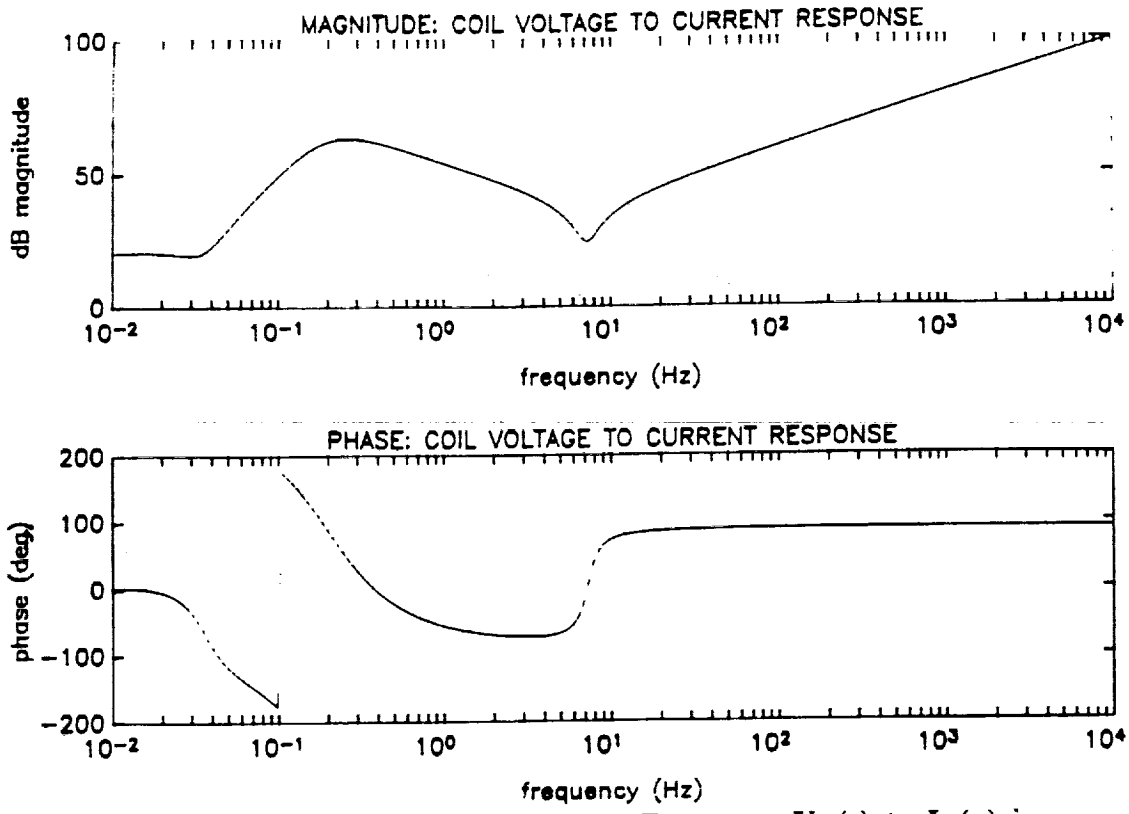

Figure 2-8. Bode Plots of the Response $V_a(s)$ to $I_a(s)$

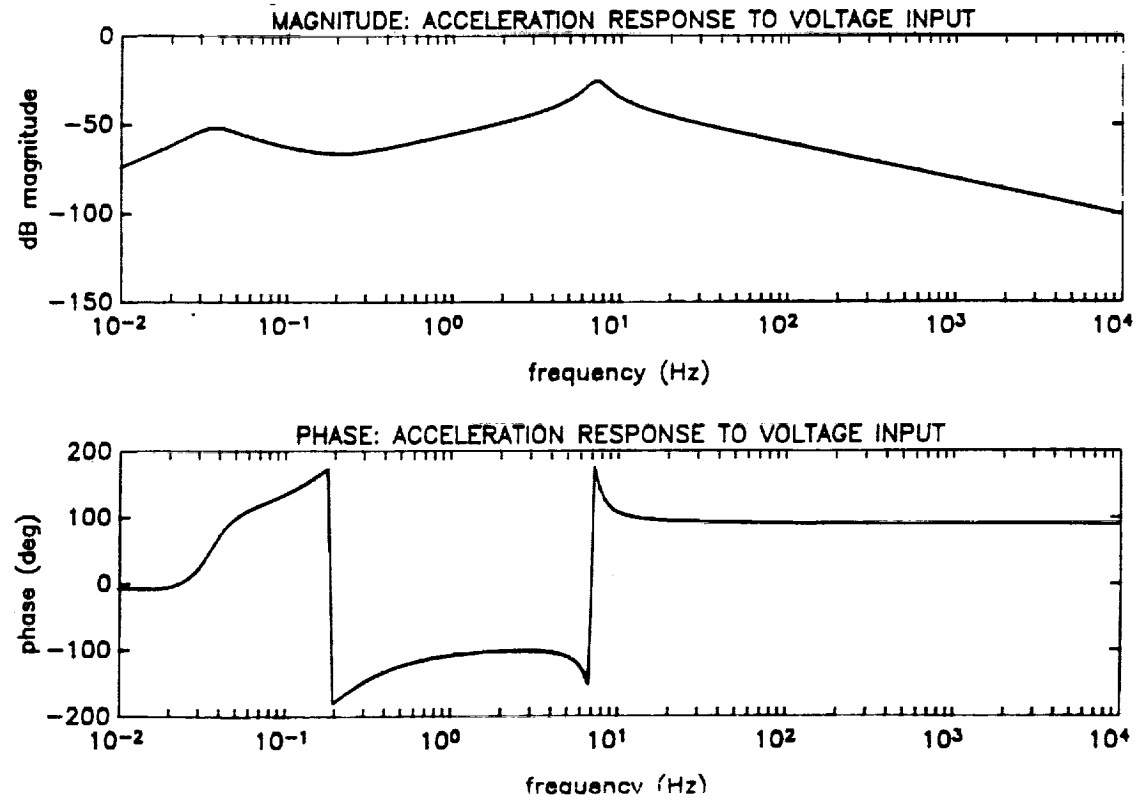

Figure 2-9. Acceleration Response of Actuator Payload System to Voltage Input

2.4 The Stiction Problem

As mentioned in the previous section, there is coulombic friction which acts between the moving actuator coil and the inner conductor. This friction can cause the moving actuator coil to "stick" at the extremes of the travel.

Several methods for reducing this friction have been proposed and tested. In one configuration the moving actuator coil spool was fabricated out of polycarbonate, and the inner connector was polished to a fine tolerance. In another configuration the polycarbonate spool was replaced with a spool which employed Teflon bushings. A third solution involved coating the inner conductor with a ceramic material. A high frequency "dither" can be added to the actuator command signal in order to reduce the stiction, but this method involves introducing disturbances to the system. It was found through iteration that the most effective means for reducing the stiction was to introduce an integral air bearing to the moving actuator coil spool. This concept is illustrated in Figure 2-10.

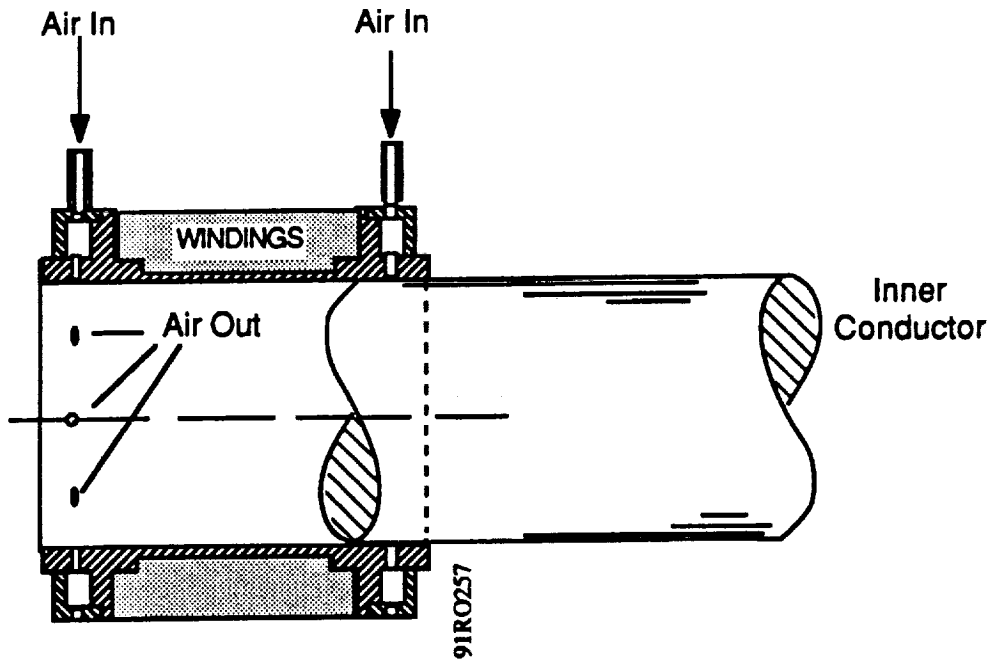

Figure 2-10. Moving Actuator Coil Spool Employing Integral Air Bearing

2.5 Other Design Considerations

The wire gage used on the moving actuator coil must be large enough to carry the required current without burning. On the other hand, lower gage (higher diameter) wire must be wound

with greater tension, which can warp the spool. If the spool is warped it will not slide freely on the inner conductor.

As the mass of the coil increases, more air must be forced through the air bearing in order to overcome the gravitational force. If the flowrate of air is not sufficient, then the weight of the coil will cause it to rest on the top surface of the inner connector.

2.6 Final Design Configuration

A schematic of the final design of the linear inertial actuator is presented in Figure 2-11. The design considerations described in Sections 2.3 through 2.5 were accommodated by using 550 turns of 26 AWG insulated magnet wire. This wire gage can be used to carry amperage in excess of 1.5 Amps, and the maximum current deliverable by the drive electronics is about 1.0 Amps.

The resulting mass of the moving actuator coil measured 0.12 kg. The force constant of the actuator is roughly 2.0 Newtons/Amp. At the maximum current available from the drive electronics, the peak force output is about 2 Newtons. A brief summary of the actuator specifications is presented in Table 2-1.

Table 2-1. Brief Summary of Actuator Specifications

Size:	7.20' (18.3 cm) Long x 3.43 [8.70 cm] High
Weight:	8.1 lb [3.7 kg]
Force Constant:	Composite Coil Form 0.5 N/A
	Air Bearing 0.5 - 1 N/A
Stroke:	±2.0" [±5.1 cm]
Frequency Response:	0 - 500 Hz
Peak Force:	Composite Coil Form 2N
	Air Bearing Coil Form >2N

A circuit diagram of the actuator electronics is presented in Figure 2-12. The moving actuator coil is shown in the lower right-hand corner of Figure 2-12. The electronics directly above the moving coil stage are the coil position caging circuitry. The current amplifier resides in the upper right-hand corner of the diagram. The circuitry in the upper left-hand corner is a modulation oscillator used in the coil position caging process.

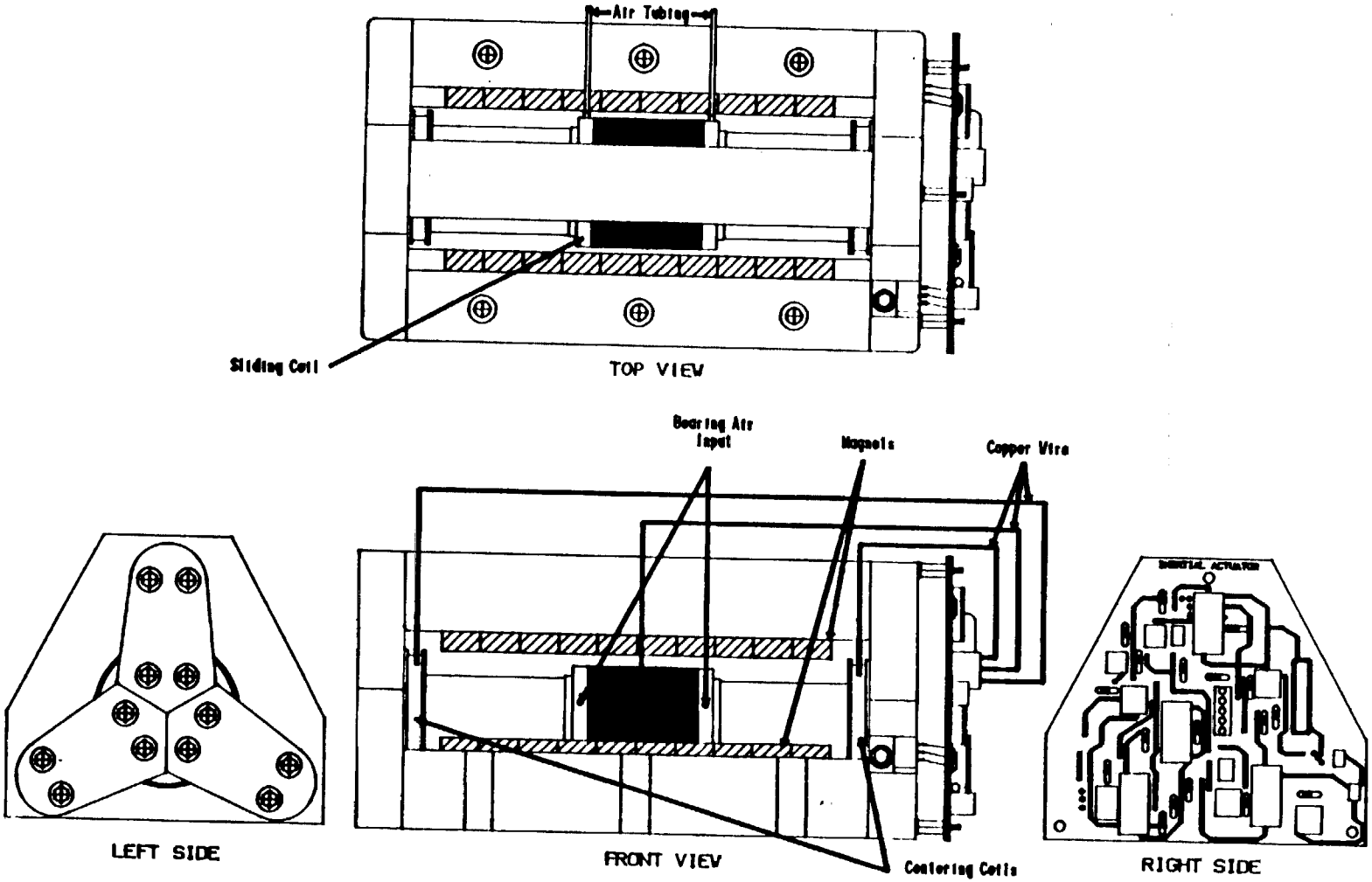

Figure 2-11. Final Actuator Design Configuration

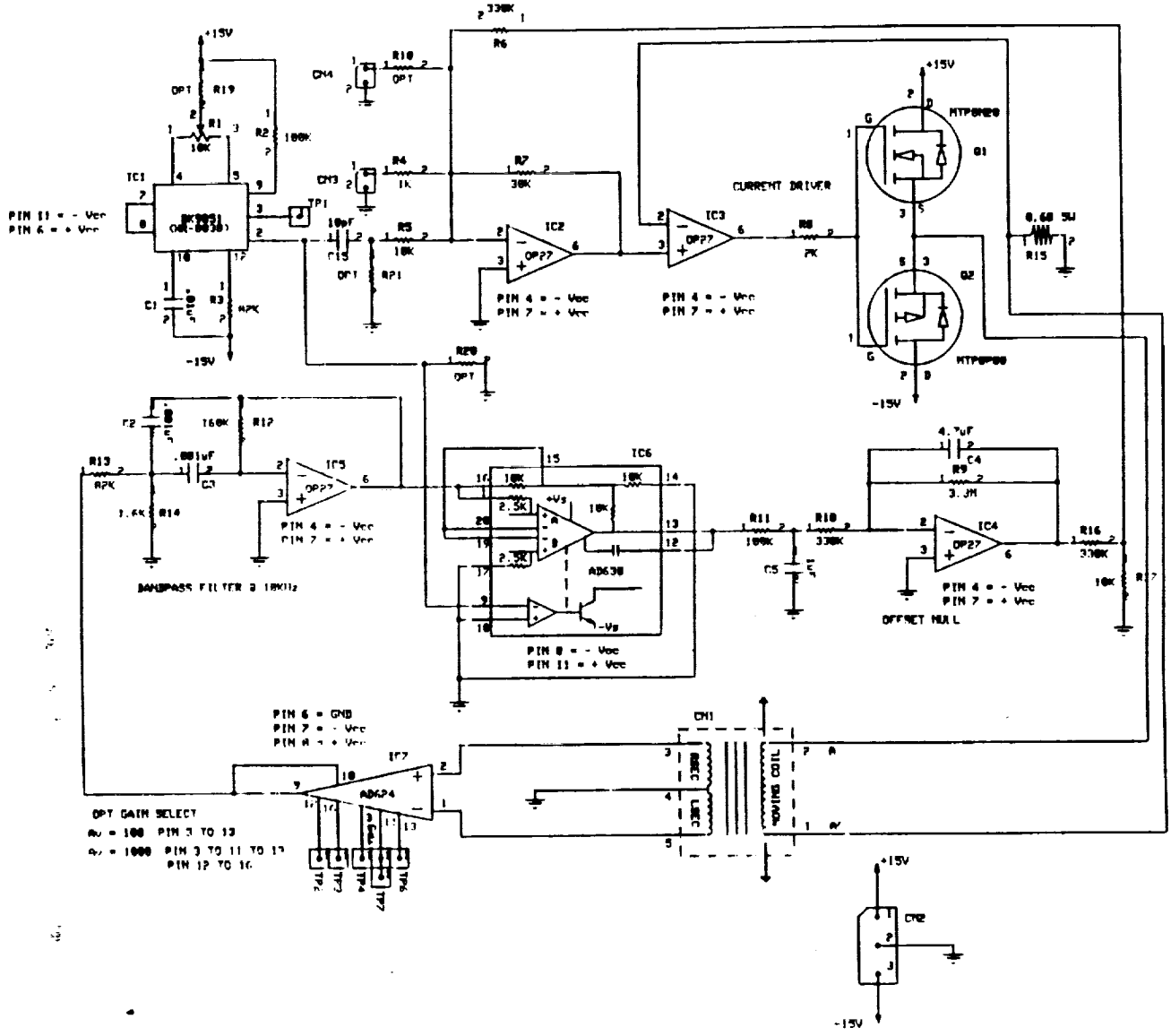

Figure 2-12. Actuator Control Electrical Schematic

3.0 CONTROL SYSTEM ACCELEROMETER SELECTION

3.1 Sensor Selection Criteria

The selection of the inertial accelerometers used in the 1DOF and 3DOF vibration isolation experiments was based on the transfer functions and the noise floors associated with the candidate sensors.

The transfer function of a given sensor contains information about the phase loss, scale factor and useable frequency range. Excessive phase loss can lead to instabilities in the closed-loop control systems. In fact, the bandwidths of the control systems have been dictated by the available phase margins, and the majority of the phase loss in the open-loop control systems has been attributed to the sensors.

The noise floor associated with a given sensor provides a measure of the smallest excitation which that sensor can measure reliably, as a function of frequency. The noise floor is generally presented as a power spectral density (psd) function. In the frequency band of control, the amplitude of the noise floor psd must be lower in amplitude than that of the disturbances that are to be rejected by the vibration isolation control system.

3.2 Candidate Sensors

There is a limited selection of affordable inertial accelerometers to choose from, which have adequate transfer functions and noise floors. ATA has evaluated many sensors over the years, and has identified several sensors which are suited for this type of application. It should be noted that the research that ATA has performed in this area has not been exhaustive. There may well be a number of sensors on the market which are well suited for this application, and are not mentioned in this section. Three sensors which ATA has evaluated are discussed below.

3.2.1 Endevco 7751-500

The Endevco 7751-500 is a piezoelectric, linear, inertial accelerometer. The operating principle of this sensor is illustrated in Figure 3-1. The motion of the case Z_0, causes the motion z, of the inertial mass, m. The motion of the inertial mass elastically deforms the piezoelectric crystal, creating a charge buildup on the faces of the crystal. This charge is then converted to a voltage signal, which is proportional to the acceleration of the case.

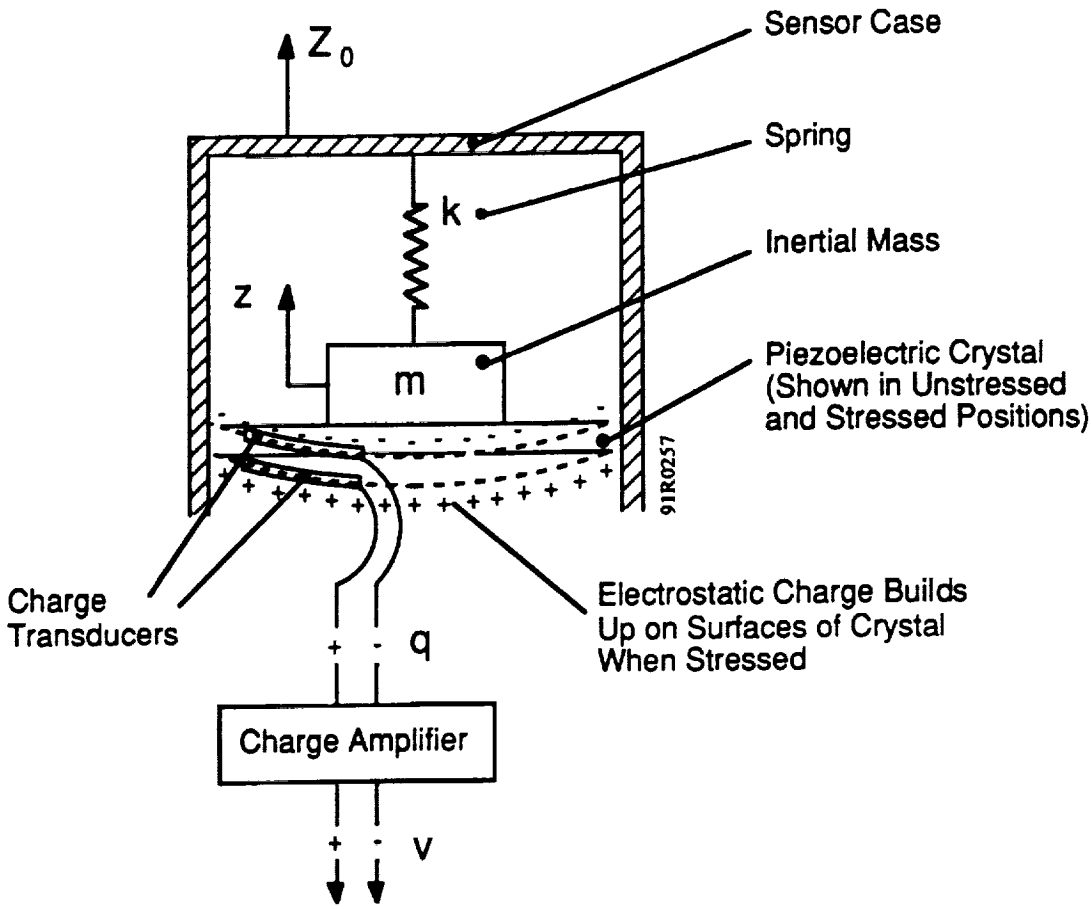

Figure 3-1. Operating Principle of Endevco 7751-500 Accelerometer

Flicker noise, often called "1/f noise" prevents the 7751-500 from measuring excitations having frequency components below about 0.1 Hz. For this reason, a highpass filter has been added to the electronics to attenuate the response of this sensor below about 0.5 Hz. Above 0.5 Hz the sensor transfer function is essentially "flat" (equal to a constant over frequency) out to 5000 Hz. This sensor has a scale factor of about 0.5 V/g.

The magnitude of the transfer function is presented in the calibration sheet provided by the manufacturer. An example calibration sheet is shown in Figure 3-2. The magnitude function is presented here in terms of the percent deviation from the nominal scale factor, between 5 and 2000 Hz. At higher frequency the actual magnitude is shown in units of dB. The peaks above 10 kHz are the mechanical resonance of the sensor.

The phase behavior and noise floor of this sensor were measured by ATA, and are presented in Figures 3-3 and 3-4, respectively.

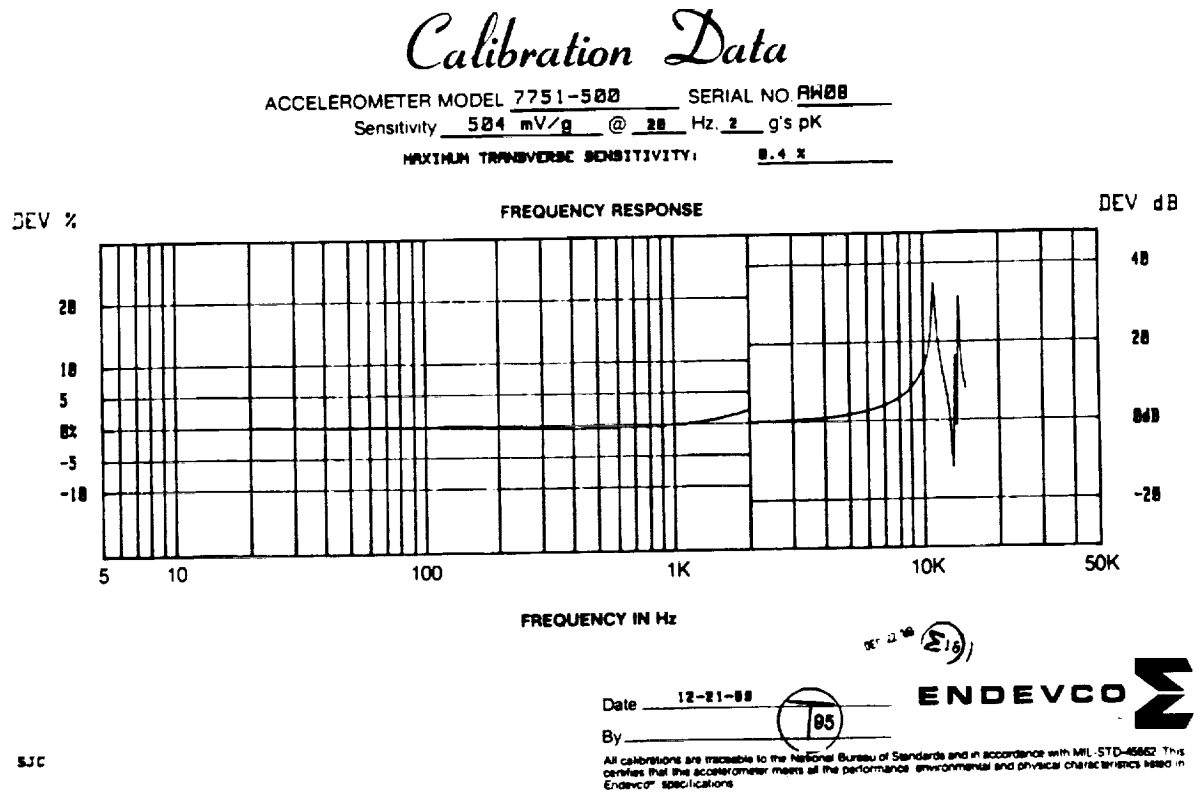

Figure 3-2. Example of an Endevco 7751-500 Calibration Sheet

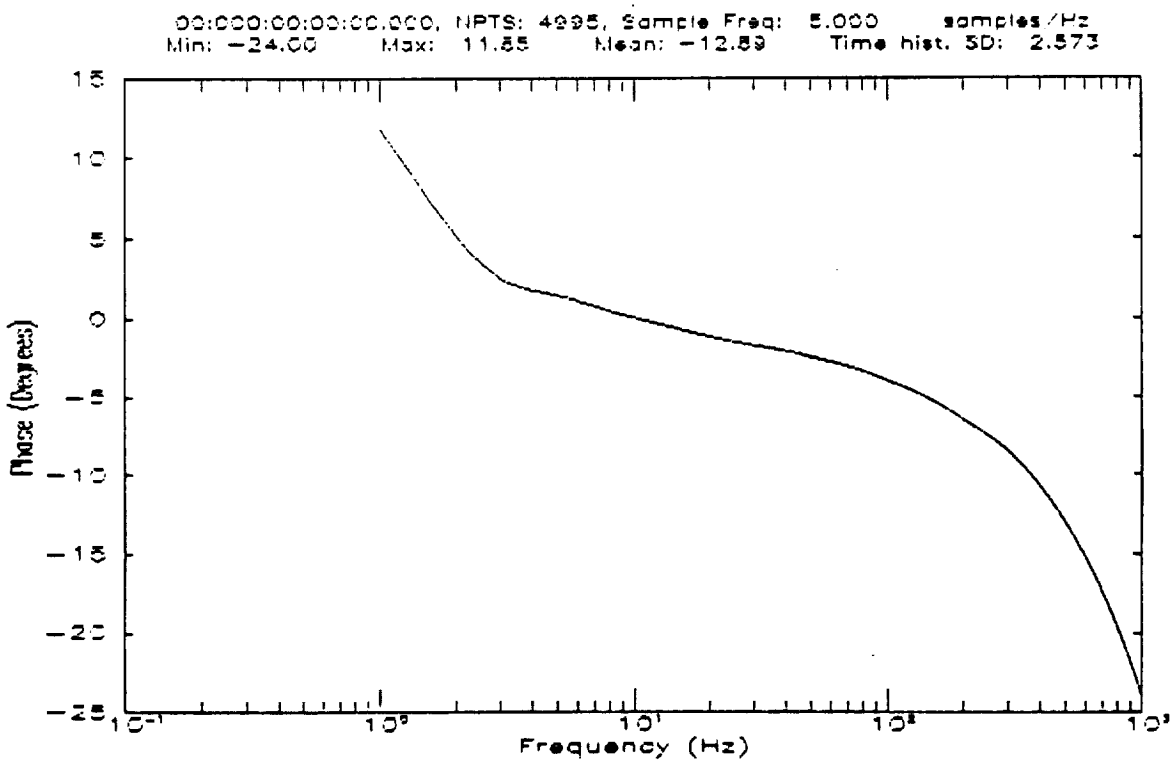

Figure 3-3. Phase Response of an Endevco 7751-500 Linear Accelerometer

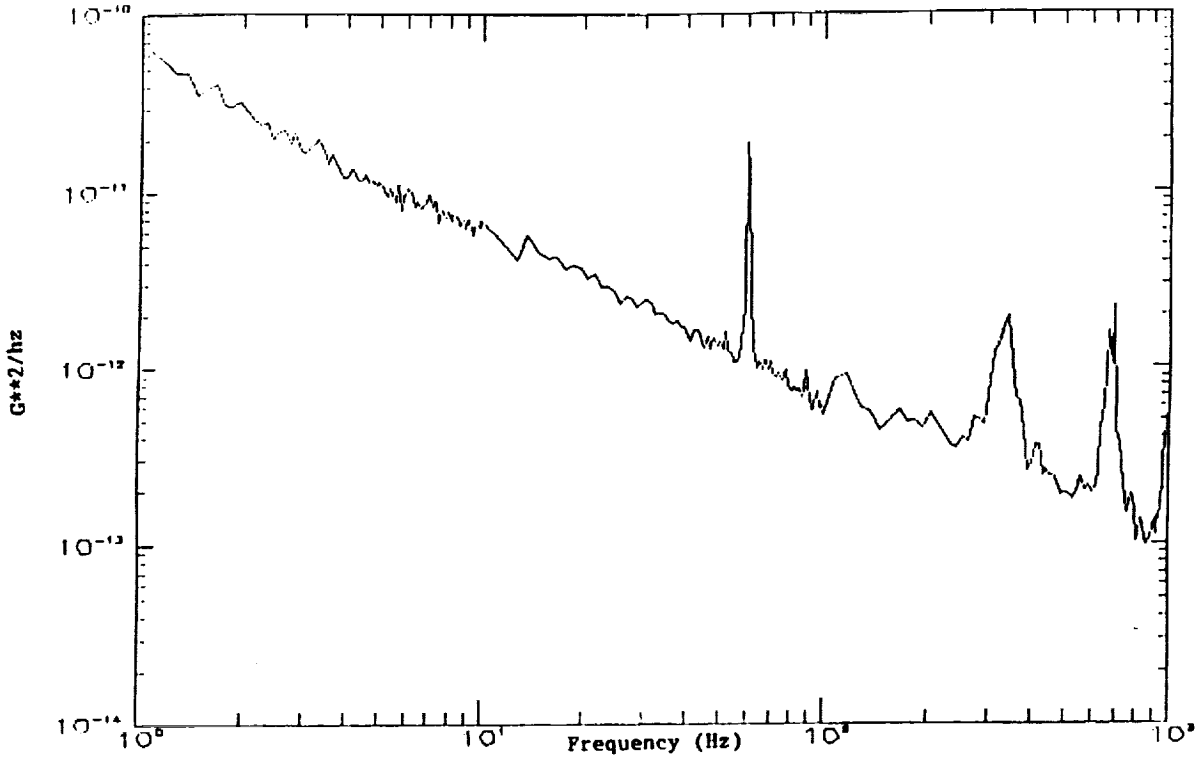

Figure 3-4. Noise Floor of an Endevco 7751-500 Linear Accelerometer

3.2.2 Teledyne-Geotech S-500

The Teledyne-Geotech S-500 is an inertial, linear accelerometer. The basic elements of this accelerometer are a spring-suspended mass and a sensor to sense motion between this mass and the sensor case. Figure 3-5 provides an intuitive illustration of the operating principle. The motion of the case Z_0 causes the motion z, of the inertial mass. The position sensor measures the relative displacement of the case and the inertial mass, m. The signal positioning then derives from the relative position measurement, a signal which is proportional to the acceleration of the sensor case.

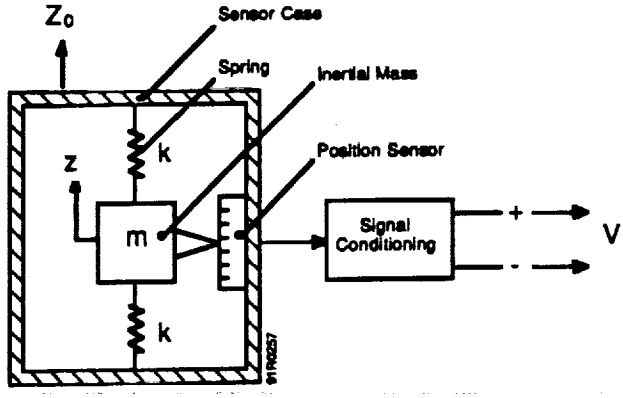

Figure 3-5. Operating Principle of Teledyne-Geotech S-500

The frequency response (transfer function) of this sensor is presented in Figure 3-6. The noise floor of this sensor was measured by ATA, and is shown in Figure 3-7.

3.2.3 Sunstrand QA-2000

The Sunstrand QA-2000 is a inertial, linear accelerometer which functions on an electromagnetic principle. Figure 3-8 provides and intuitive illustration of the operating principle. The inertial mass is composed of a magnetized material, and produces around itself, a magnetic field. An opposing magnetic field is produced by a coil beneath the inertial mass. The intensity of the opposing magnetic field is controlled by varying the current in the coil. The inertial mass is supported by the repulsion between the permanent and controlled magnetic fields. A position sensor measures the relative displacement of the inertial mass and the sensor case. When the sensor case accelerates, the relative displacement between the inertial mass and the case, Z_0-z changes. The current in the coil is continuously adjusted in a closed loop, such that the repulsive magnetic force restores the relative displacement to a null reading. By altering the current in the coil, the inertial mass is held fixed with respect to the sensor case (to within some tolerance). Therefore, the current required to maintain this condition, is at all times proportional to the acceleration of the case. The voltage drop across a resistor in the coil circuit is used to back out a voltage signal, which is proportional to the current by Ohm's Law.

Bode plots of the frequency response (transfer function) of this sensor were generated by ATA, and are shown in Figure 3-9. The peaks at high frequency are caused by the test apparatus, and not by the sensor itself. The phase loss however, is caused by the sensor.

The noise floor of the QA-2000 has been measured by ATA over a limited frequency band. The measured noise floor is presented in Figure 3-10.

3.3 Comparison of Sensor Performances

The performance goal of the vibration isolation system was presented in Figure 1-2. It is desirable to employ a sensor having a noise floor that is at least an order of magnitude below the smallest disturbance to be rejected. Thus, if at some frequency the performance goal is 1 micro-g, then the level of the noise floor should be at most, 0.1 micro-g. This requirement specifies a performance curve for the sensor noise. In Figure 3-11 the platform performance goal, the sensor noise goal, and the noise floors discussed above are presented on the same plot.

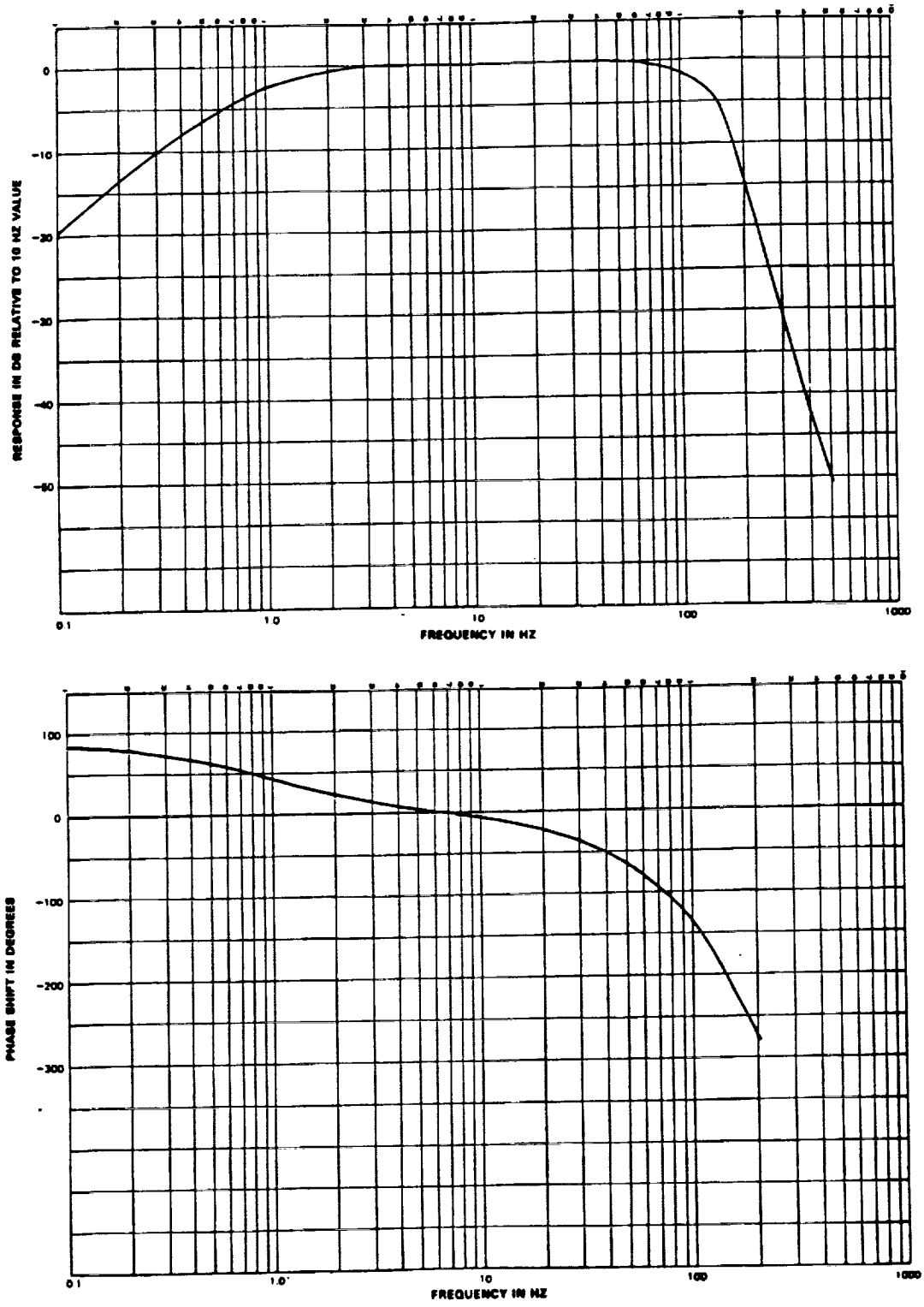

Figure 3-6. Transfer Function Magnitude and Phase Functions for the Teledyne-Geotech S-500

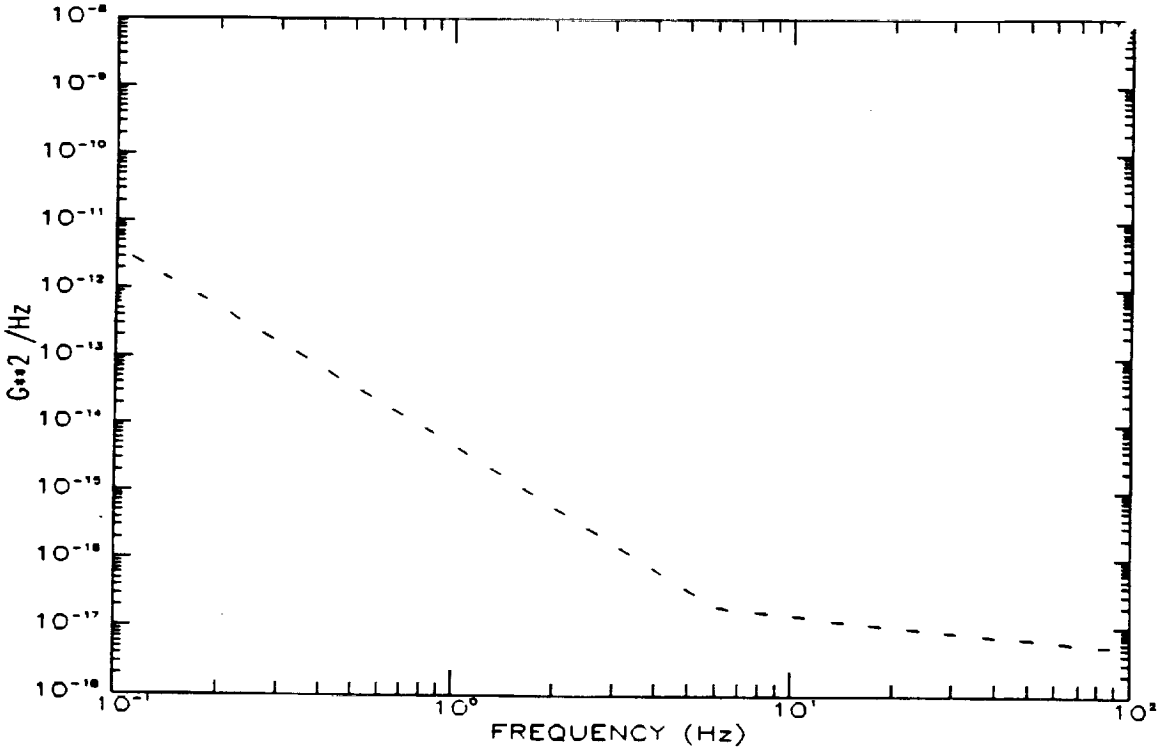

Figure 3-7. Noise Floor of Teledyne-Geotech S-500

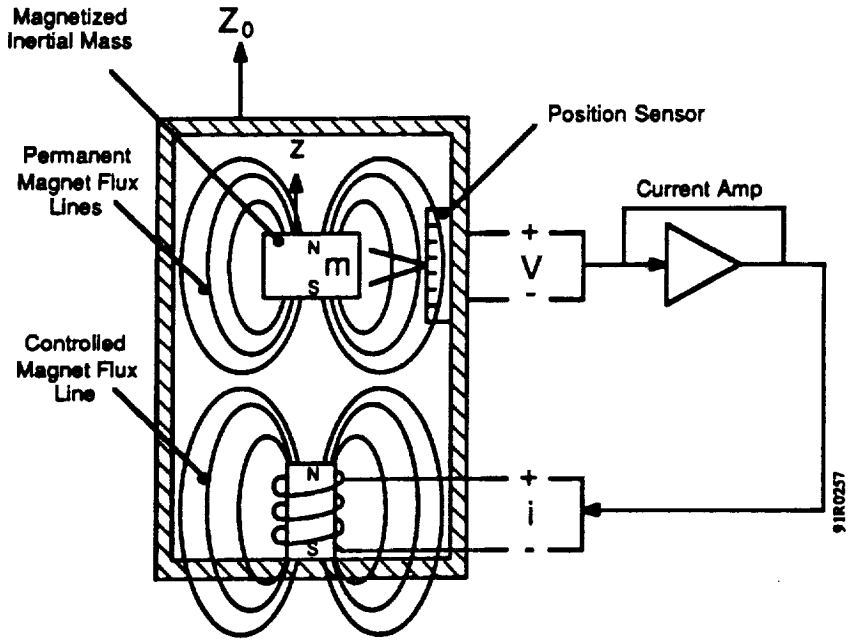

Figure 3-8. Conceptual Illustration of QA-2000 Operating Principle

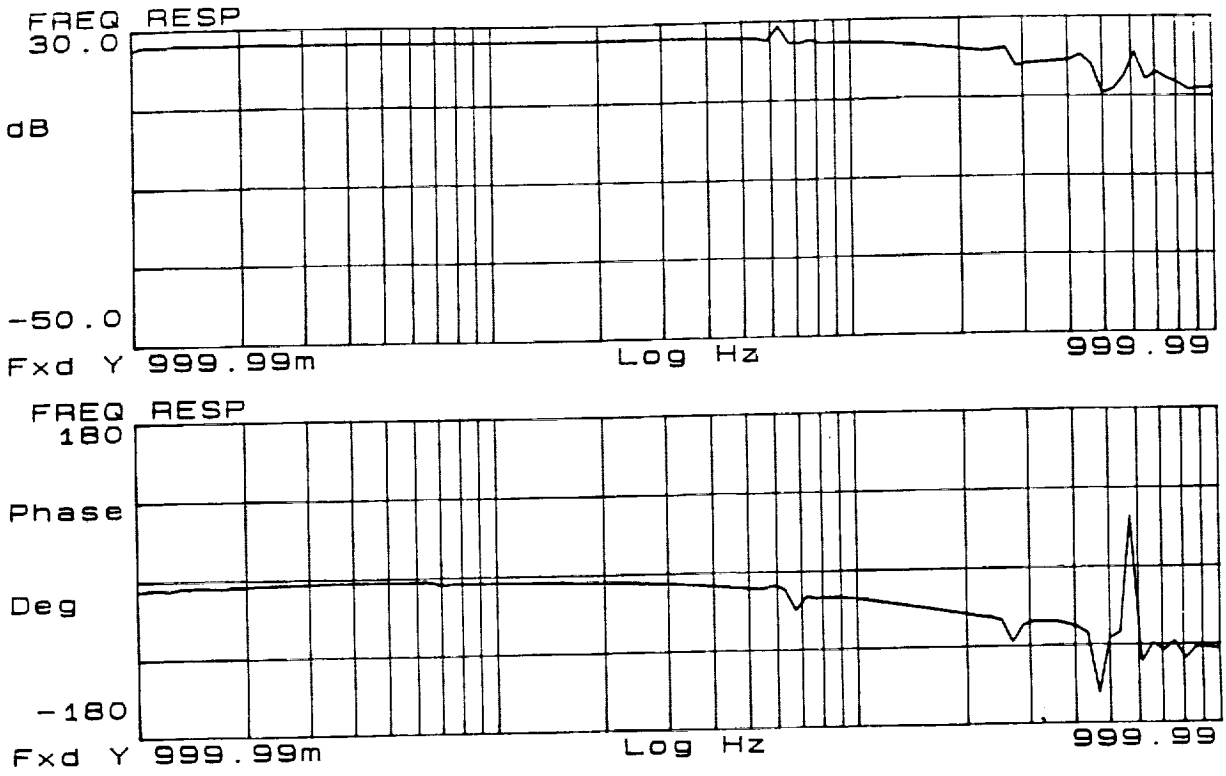

Figure 3-9. Bode Plots of the QA-2000 Frequency Response

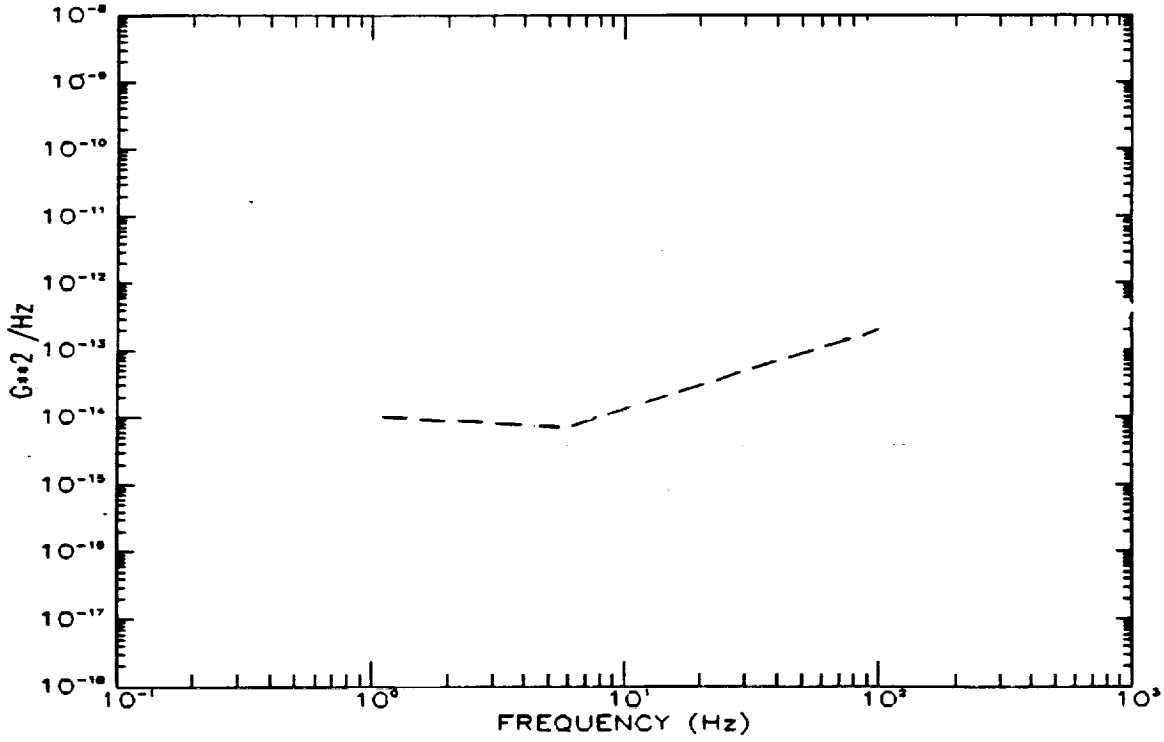

Figure 3-10. Noise Floor of the Sunstrand QA-2000

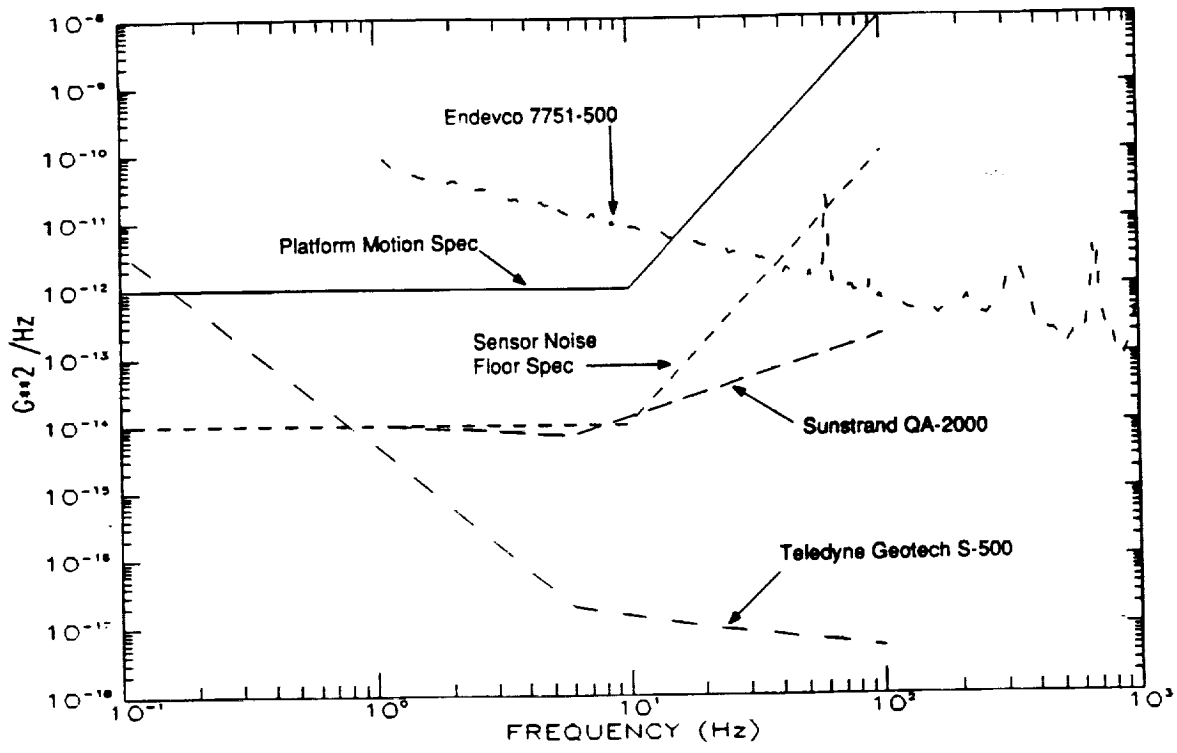

Figure 3-11. Comparison of Sensor Noise Floors

The most impressive noise floor is that associated with the Teledyne-Geotech S-500. However, this sensor causes an unacceptable phase loss in the open-loop control system response. The magnitude response is attenuated at -80 dB/decade. It is possible to implement a digital filter which "flattens out" the response above 100 Hz, in order to improve the phase behavior. However, this filter must be implemented in the Digital Signal Processor (DSP), where it consumes limited computation time. In addition, the coefficients of the required digital filter are large because of the relatively high frequency corner (100 Hz), and the order of the polynomials. The DSP does not operate correctly when the coefficients of the difference equations become too large. An analog implementation of the filter is difficult to implement with acceptable noise performance.

An alternative to the corrective filter is to alter the electronics of the S-500 itself. The mechanical dynamics of the sensor create an attenuation of only -40 dB/decade above 100 Hz. The other two orders of rolloff are due to a second-order lowpass filter at 110 Hz. This filter is added (by Teledyne-Geotech) because the mechanical resonance has an unpredictable amount of peaking, which is undesirable from a marketing standpoint. The lowpass filter can be removed, which

would simplify the corrective filter from fourth-order to second-order. Unfortunately, the cost and schedule delays associated with this modification were unacceptable.

The Sunstrand QA-2000 exhibits an acceptable noise floor as well. The phase loss associated with the QA-2000 is also acceptable. Unfortunately large bias errors are inherent in the signals generated by this sensor.

The Sunstrand QA-2000 sensor was used in the control of the 1DOF system. The bias errors were removed by external electronics before the signal entered the DSP. However, more sensors were required to control the 3DOF system, and electronics were not available to condition all of the sensor outputs in this system. For this reason, Endevco 7751-500 sensors were employed in the 3DOF system.

4.0 SINGLE-AXIS (1DOF) VIBRATION ISOLATION SYSTEM DEVELOPMENT

4.1 Simulation of Orbiter Environments

The linear inertial actuator was developed for space-based experiments, and thus it made sense to demonstrate the performance of the actuator in a vibration environment similar to that experienced on orbiting spacecraft. When contrasted with ground-based experiment environments, the most pronounced characteristic of the space environment is the absence of the 1-g acceleration vector, directed radially toward the center of the earth.

There are many approaches to the simulation of space environments, ranging from neutral buoyancy floatation to parabolic aircraft trajectories. The most affordable schemes simulate "weightlessness" in fewer than six axes. Examples include magnetic suspension systems and air bearing tables.

The linear inertial actuators themselves have significant mass (about 8 pounds per actuator), and other peripheral hardware having substantial mass is required to realize the isolation system. Magnetic suspension systems become increasingly expensive, and draw larger supply currents as the weight of the payload increases.

After evaluating the alternatives, ATA engineers elected to perform tests to verify the feasibility of employing air bearing tables to simulate space environments. The objective of the testing was to show that the disturbances induced by the air bearing could be rejected by the control system.

The Physics Department of the University of New Mexico uses a single-rail, linear air bearing table for classroom demonstrations. It was assumed that ATA could fabricate a precision air bearing table employing two parallel rails, which would be more quiet, and could support more weight. Results from tests performed on the single-rail air bearing (owned by the University) could then be treated as a "worst-case" disturbance environment. ATA engineers instrumented a carriage which floats on the single-rail air bearing with linear accelerometers. Power spectral density (psd) functions of the motion experienced on the floated carriage were obtained in order to determine the amplitude of the disturbances as a function of frequency. In these tests two sensors were mounted back-to-back on the air bearing carriage, in-line with the air bearing rail. This configuration is shown in Figure 4-1.

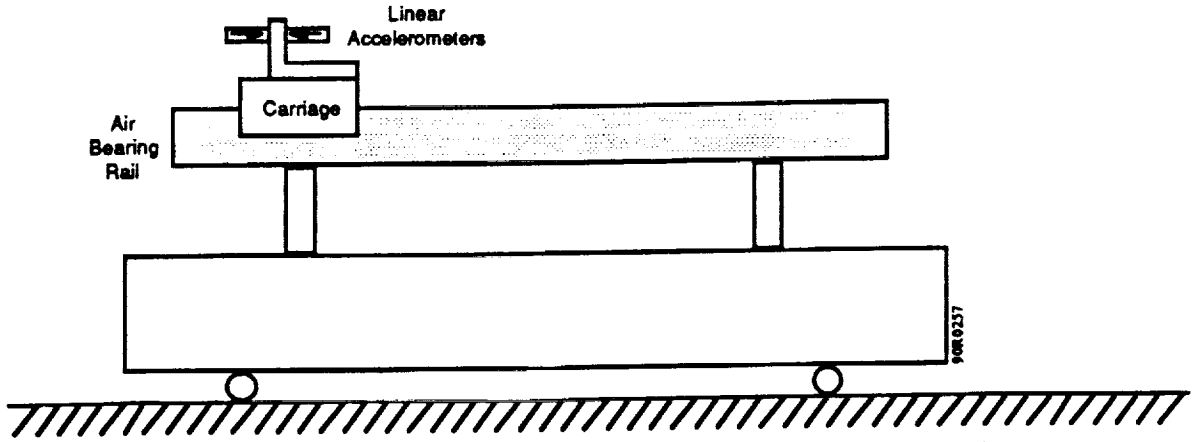

Figure 4-1. Single-Rail Air Bearing Test Configuration

The coherent power psd[4] associated with both back-to-back sensors are overlaid in Figure 4-2. The platform motion specification line discussed in Section 1 is also included in Figure 4-2. Comparison of these results to the specification line dictated that rejection of between 20 and 30 dB would be necessary to negate the disturbances. This requirement seemed reasonable, and air bearings were then selected as the mechanism for the simulation of the space environment.

4.2 Single-Axis (1-DOF) Air Bearing Table Configuration

A dual-rail air bearing table was designed and fabricated in order to simulate "weightlessness" in a single horizontal axis. The configuration of this table is shown in Figure 4-3. One of the rails is turned up on end such that the contact between the rail and the skate is triangular. The other rail/skate interface is flat. This configuration prevents motion in other axes. The two rails are attached to a welded steel frame with adjustable alignment screws. Adjustable feet provide additional leveling capability.

Air is supplied to the table by an electric ring compressor. The compressor requires three-phase power, and is capable of delivering up to 150 cubic feet of air per minute.

The actuators, sensors and other support electronics are mounted on the carriage. The digital signal processor (DSP) boards are mounted in a card cage, which is in turn fastened to the bottom of the carriage.

---

4 A discussion of the signal processing techniques employed in the DAMPER effort is provided in the ATA report "Digital Active Materials Processing Experiment (DAMPER) Transfer Function Determination, February, 1991.

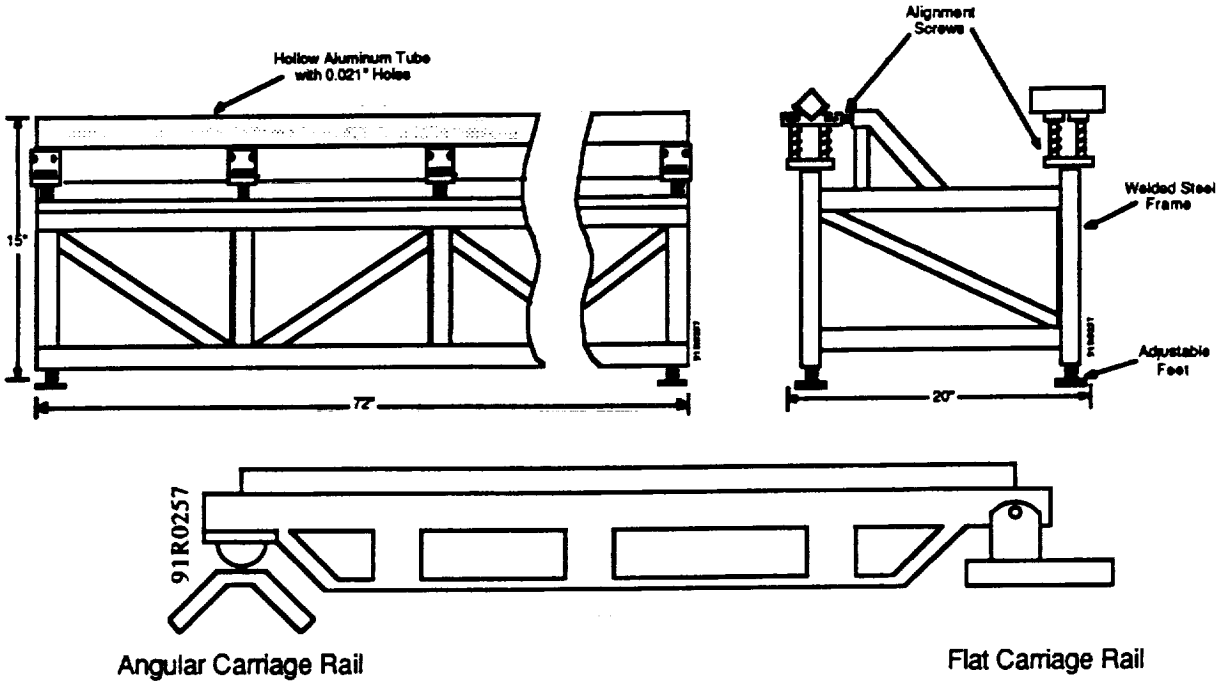

Figure 4-3. a) Side View of Single-Axis Air Bearing Table, b) Front View, c) Front View of Carriage

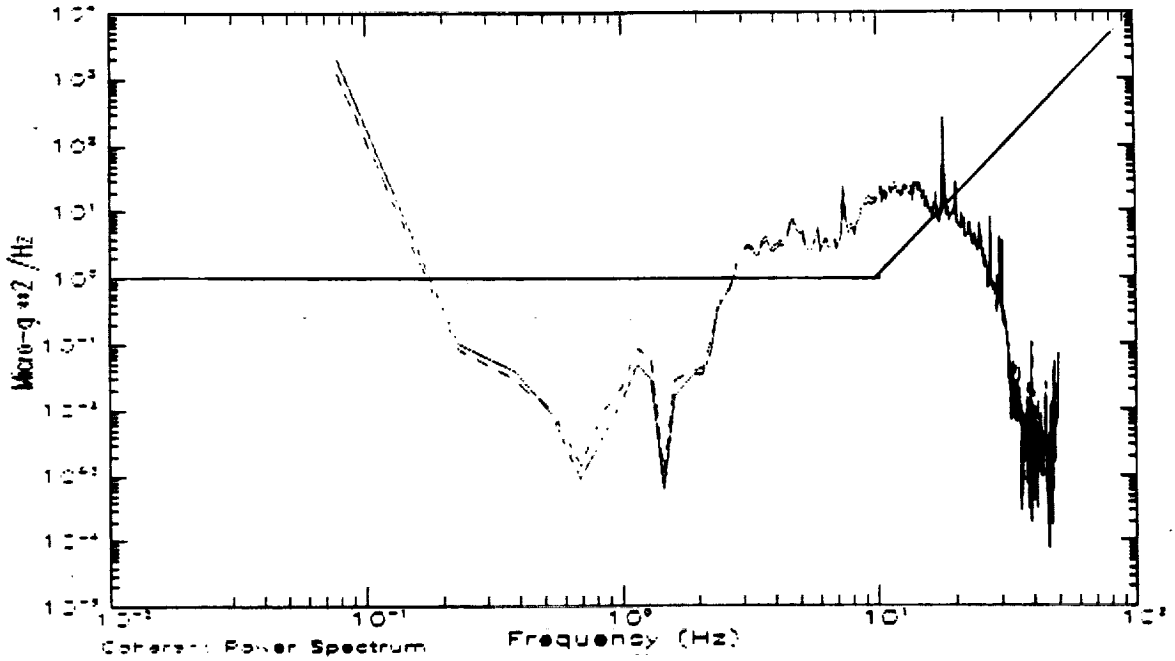

Figure 4-2. Coherent Power PSD from Two Redundant Sensors, Mounted on Floated Air Bearing Carriage, In-Line with Bearing

4.3 Single-Axis (1DOF) Vibration Isolation Control System

A block diagram of the 1DOF vibration isolation control system is shown in Figure 4-4. The reference input is zero, because it is desired to minimize platform motion. The transfer function which describes the carriage acceleration due to an actuator force input is labeled as the "plant" in Figure 4-4. This function is climbing at 2 orders of magnitude per decade at frequencies below the mechanical resonance of the system. At frequencies between the mechanical resonance and the first structural resonance of the carriage, this function is flat. There is a slight "dip" in the air bearing rails in which the carriage seeks equilibrium. The spring force which dictates the frequency of the mechanical resonance is produced by the gravitational attraction to that equilibrium point. The mechanical resonance is roughly 1.0 Hz.

The actuator has a flat response between 0.1 and 500 Hz. Below 0.1 Hz the low-frequency caging circuitry attenuates the actuator response. Above 500 Hz the response is attenuated by a second-order lowpass filter. The purpose of this filter is to prevent the excitation of modes above 500 Hz.

The Sunstrand QA-2000 accelerometer is also flat in the frequency range from 0.1 to 100 Hz (see Figure 3-9). The uncompensated, open-loop frequency response of the system is predicted in Figure 4-5. This response requires compensation because there is no defined point at which the magnitude function crosses the 0-dB line. The required compensation is a combination of a first-order lowpass filter at about 3 Hz, and a second-order lowpass filter at 30 Hz. This filter "rolls off" the response at 1 order of magnitude per decade between 3 Hz and 30 Hz, and at 3 orders of magnitude per decade at frequencies above 30 Hz. The steep roll-off above 30 Hz is required to prevent the structural resonance peaks from protruding above the 0-dB line, at frequencies at which there is no phase margin. The compensation filters are implemented as digital filters by mapping them from the continuous domain to the discrete domain. A complete discussion of this mapping is presented in the ATA report entitled "Digital Active Materials Processing Experiment (DAMPER) 1DOF Platform Development Task Final Report". The compensated, open-loop frequency response of the system is predicted in Figure 4-6.

Notice that the compensation forces the magnitude function in Figure 4-6 to cross the 0-dB line at a well defined frequency of about 13 Hz. Notice also that the phase margin at 13 Hz is acceptable.

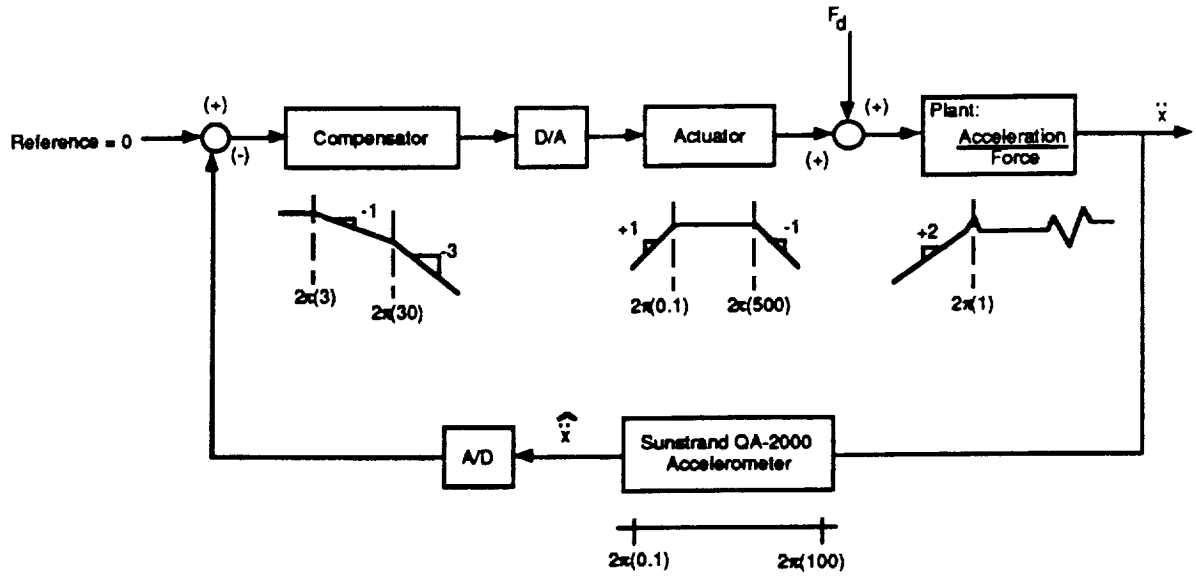

Figure 4-4. Single-Axis Vibration Isolation Control System Block Diagram

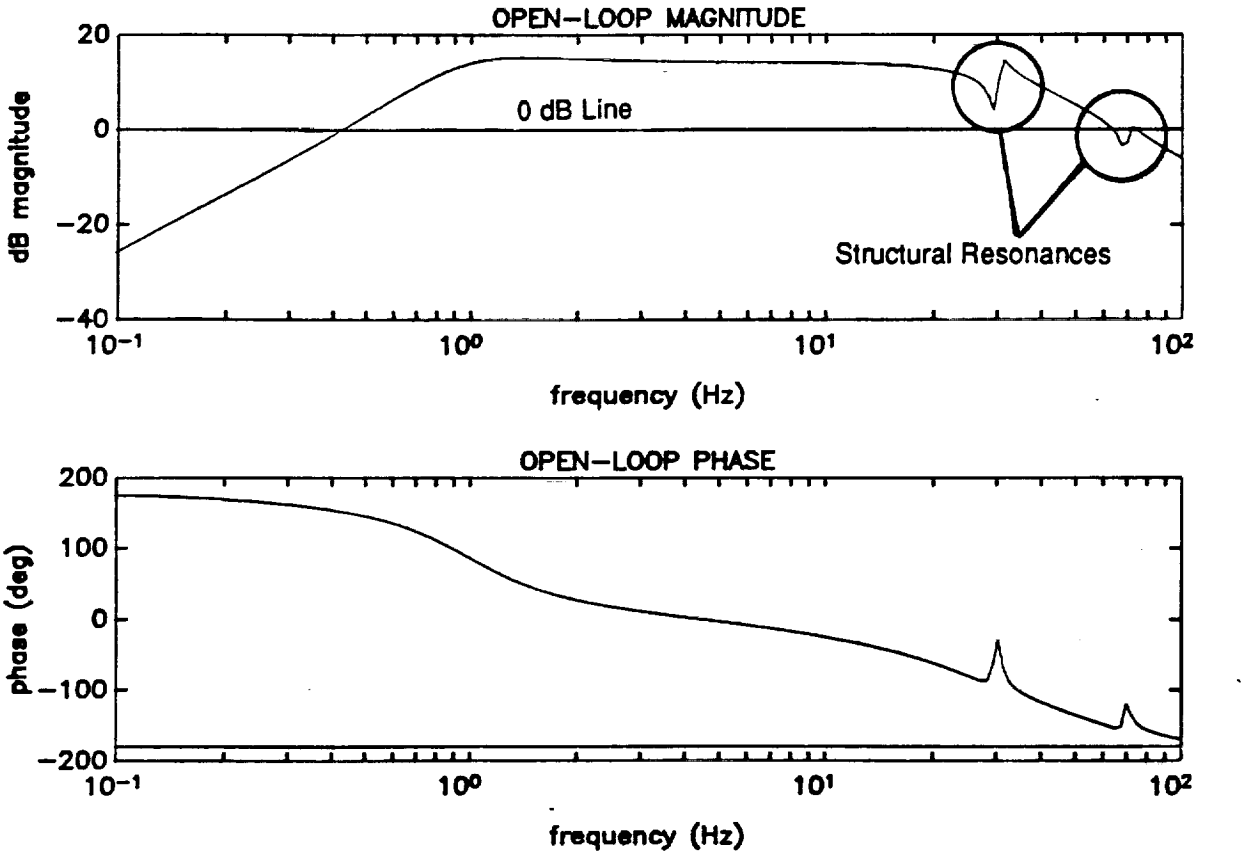

Figure 4-5. Predicted, Uncompensated Open-Loop Frequency Response of the Single-Axis Isolation Control System

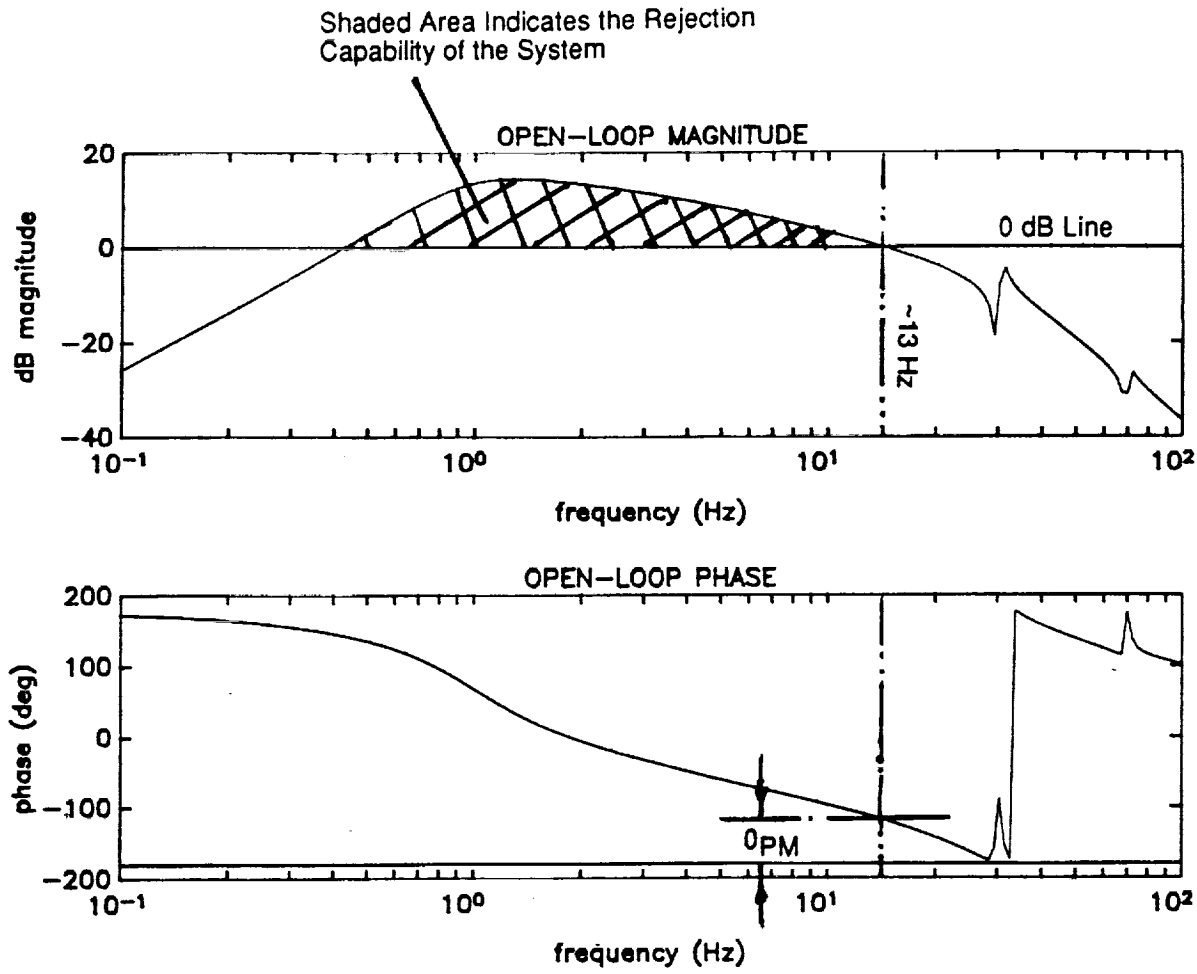

Figure 4-6. Predicted, Compensated Open-Loop Frequency Response of the Single-Axis Isolation Control System

The closed-loop response of the control system can be predicted from the response presented in Figure 4-6. With a zero-valued reference input, the closed-loop frequency response is also the error rejection function for the control system.

$$G_{cl}(jw) = G_{er}(jw) = \frac{1}{1 + G_{ol}(jw)} \tag{15}$$

The predicted closed-loop frequency response of the system is presented in Figure 4-7. At this value of the open-loop gain, the rejection is maximum at about 18 dB. However, a small amount of amplification between 0.1 and 0.5 Hz, and between 15 and 50 Hz is unavoidable. Increasing the open-loop gain will increase the rejection between 0.5 and 15 Hz, at the expense of further amplification between 0.1 and 0.5 Hz, and between 15 and 50 Hz.

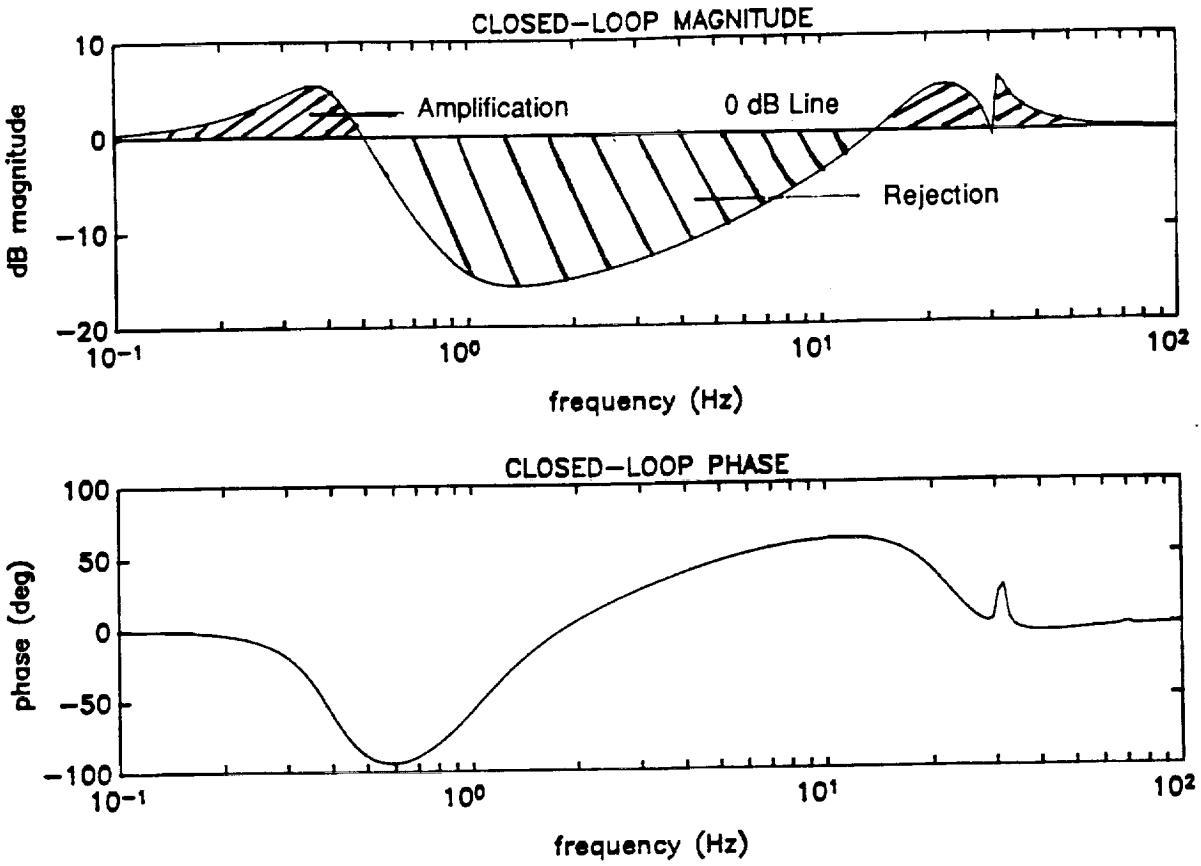

Figure 4-7. Predicted, Closed-Loop Frequency Response of the Single-Axis Isolation Control System

4.4 Single-Axis (1DOF) Vibration Isolation System Digital Electronics Hardware and Architecture

The active vibration isolation control algorithms are computed in real time using a Motorola 56001 DSP board. Figure 4-8 shows the conceptual layout of the digital electronics hardware, and the manner by which it is interfaced with other system components.

The DSP electronics consist of a set of electronics boards. The boards include the DSP itself, the analog input (A/D) and the analog output (D/A) cards. The boards are installed in a card cage on the single-axis air bearing carriage. The user communicates with the DSP from an IBM PC. The PC and DSP are interconnected by an RS-232 interface, as shown in Figure 4-8. All software development for the DSP is performed on the PC. The executable (machine language) codes required to perform the calculation of the control algorithms are obtained by translation of the DSP assembly (or C) language codes, written on the PC. The executable codes are then downloaded from the host computer (PC) to the DSP via the RS-232 interface.

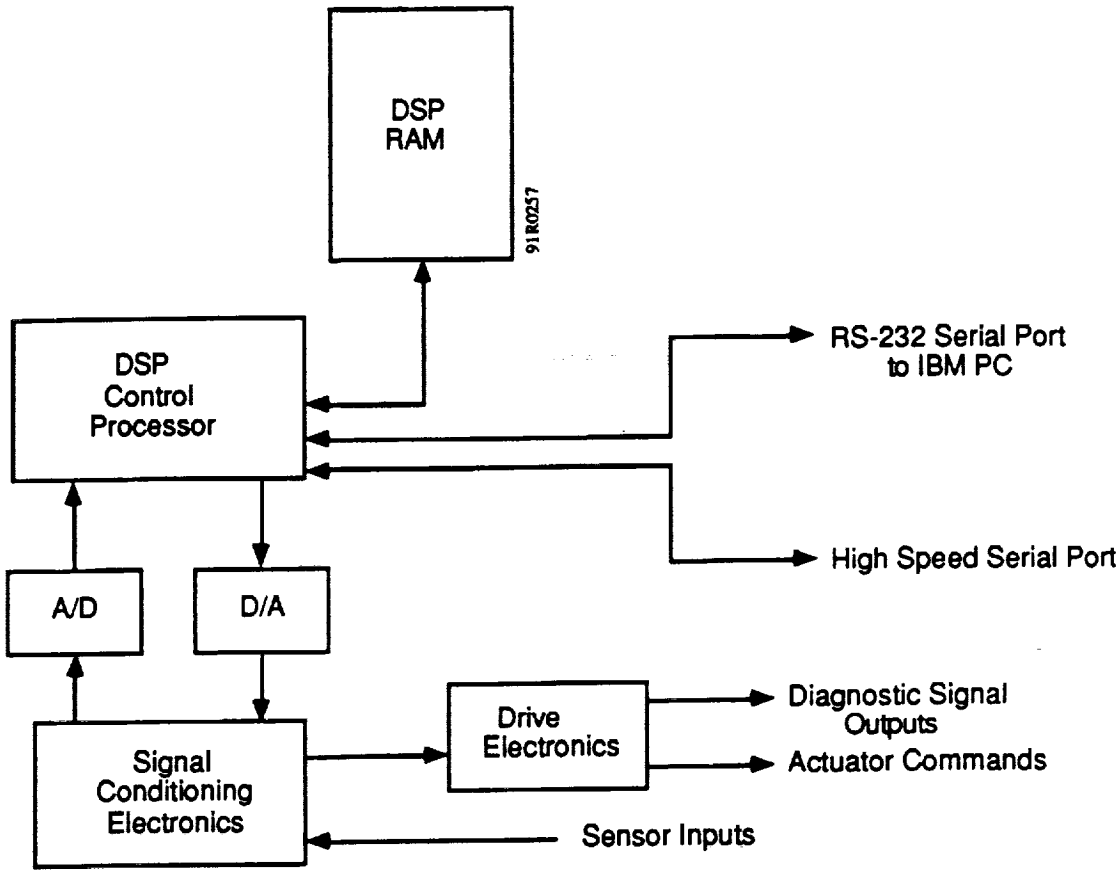

Figure 4-8. Conceptual Layout of Digital Electronics Hardware

Signal conditioning and drive electronics, external to the DSP provide the interface between the computer/DSP system, and the sensors and actuators on the platform. These electronics include (among other things) low-frequency highpass filters which are used to AC-couple (remove unwanted DC biases in) the sensor and drive signals.

5.0 RESULTS OF SINGLE-AXIS (1DOF) VIBRATION ISOLATION SYSTEM TESTING

5.1 Open-loop Transfer Function Testing

The predicted uncompensated and compensated open-loop frequency responses of the 1DOF vibration isolation system were presented in Figures 4-5 and 4-6, respectively. These figures should be compared with the measured responses presented below in Figures 5-1 and 5-2. The Bode plots of Figures 4-5 and 5-1 are in fairly good agreement. However, the phase loss depicted in Figure 5-1 is more significant than that shown in Figure 4-5. One possible explanation for the discrepancy is that the sensor drive electronics were not set up correctly when the test which produced Figure 5-1 was run. Improper wiring of Sunstrand QA-2000 accelerometers can result in unwanted phase loss. Note that the frequency locations of the structural resonances in Figures 4-5 and 4-6 are arbitrary, and that these resonances are not intended to depict modeled phenomena.

The compensated responses shown in Figures 4-6 and 5-2 are in good agreement as well. As before, the phase loss is more pronounced in the test data than it is in the model. The data presented in Figure 5-2 implies that the control loop can be closed at about 12 Hz. The resulting rejection is about 21.88 dB, which exceeds the value predicted in Figure 4-6.

5.2 Closed-loop 1DOF Control System Performance Testing

There are several methods for assessing the performance of a vibration isolation system. The first involves driving the closed-loop system, and obtaining Bode plots of the closed-loop transfer function. The result would presumably look something like the response shown in Figure 4-7.

A more direct method can be used however. A disturbance can be imposed on the payload, and a psd of the resulting motion can be acquired while the loop is inactive. This psd is then compared with a similar measurement acquired while the loop is active. The difference between the controlled and uncontrolled platform motion can then be conveniently assessed by overlaying these two psd functions on the same plot. Figure 5-3 is such a plot. The disturbance was injected by mounting a second inertial actuator in parallel with that used to abate the disturbance. The second actuator was driven with a swept sine input from the frequency analyzer while the psd functions were obtained. The actuator used to inject the disturbance was not equipped with an integral air bearing, and had a low frequency stiction problem. Consequently, the psd functions

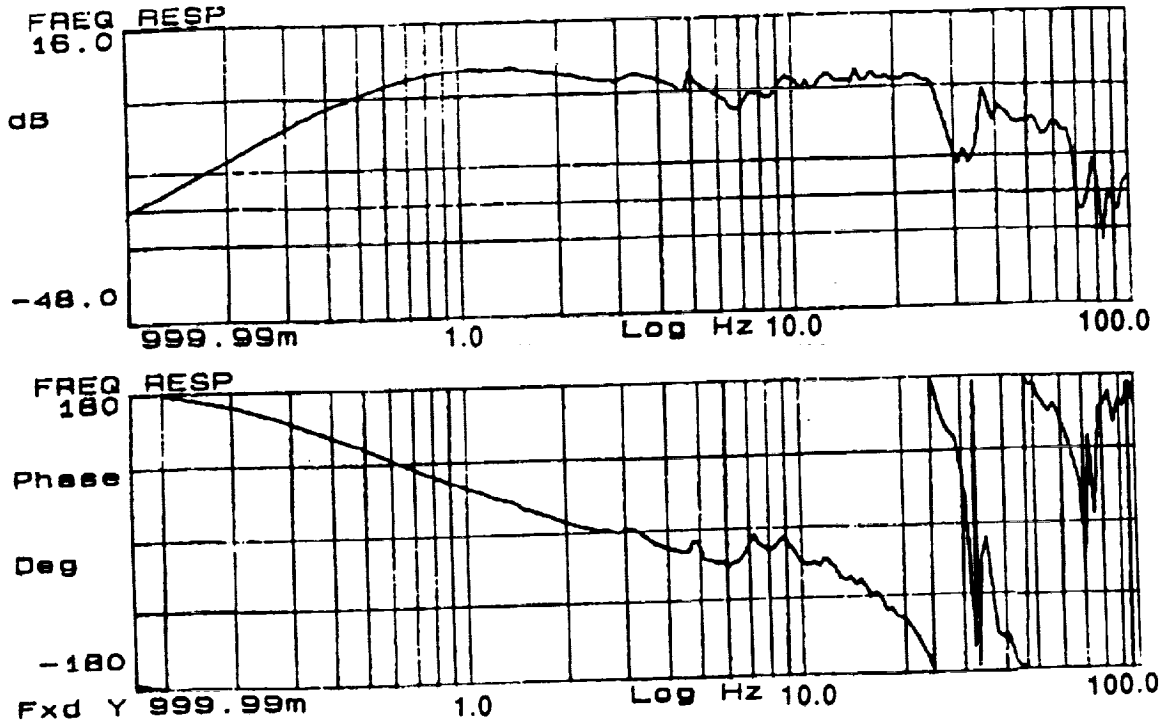

Figure 5-1. Measured, Uncompensated Open-Loop Frequency Response of Single-Axis Isolation Control System

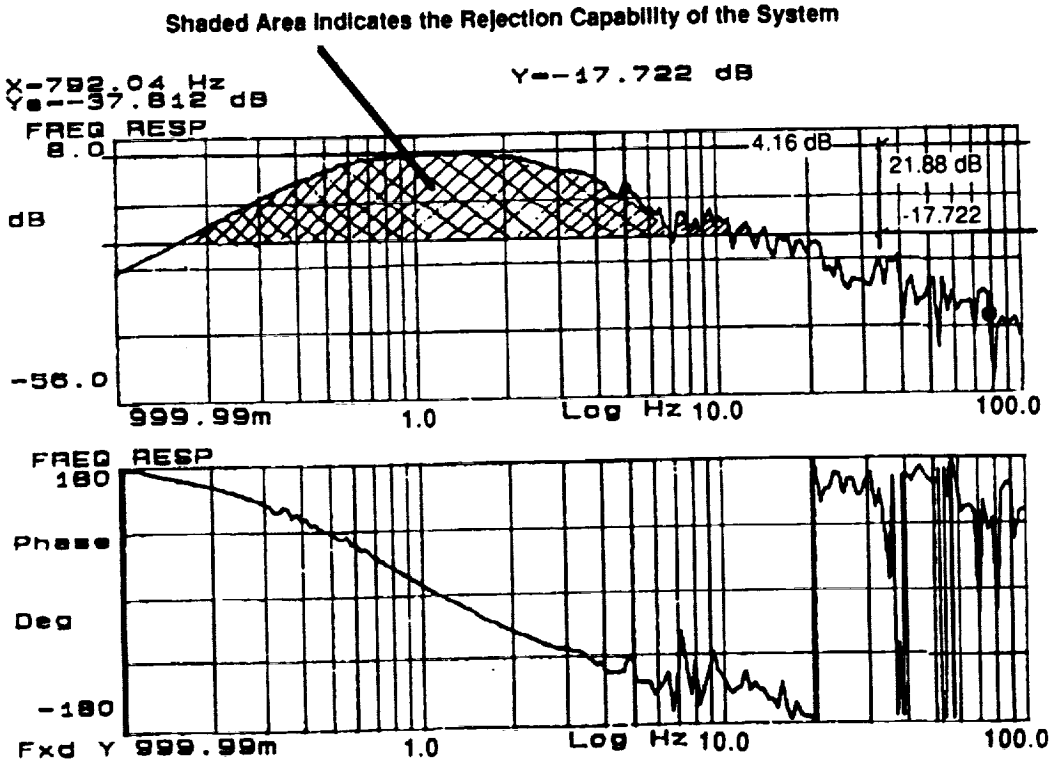

Figure 5-2. Measured, Compensated Open-Loop Frequency Response of the Single-Axis Isolation Control System

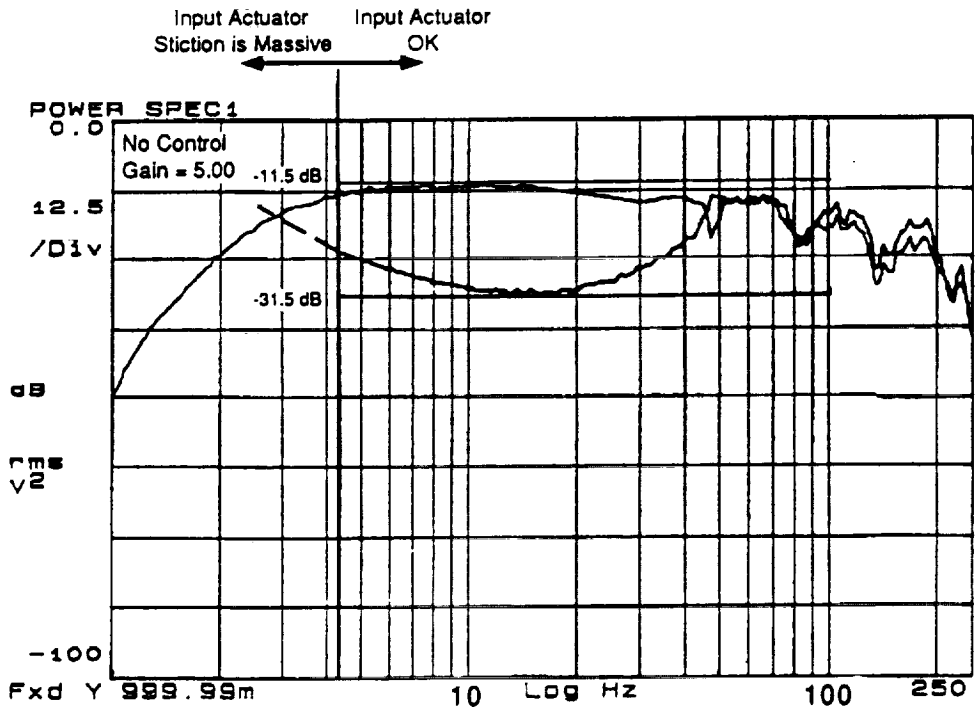

Figure 5-3. Controlled and Uncontrolled PSD Functions with Injected Disturbance

shown in Figure 5-3 are not reliable at frequencies below about 4.2 Hz. However, in the reliable frequency band of the measurement, the predicted rejection of about 20 dB was realized.

A third and final assessment of the performance of a vibration isolation control system involves acquiring the psd functions described above, without injecting a disturbance. Comparison of these measurements indicates the ability of the system to abate the ambient vibration environment. The psd functions of the payload ambient vibration (with the payload floated on the air bearing), and the payload vibration with the control loop active, are overlaid in Figure 5-4. Again, a maximum disturbance rejection of about 20 dB is apparent (note that 20 dB is one order of magnitude).

The payload vibration specification (goal) line is superimposed on the psd plots in Figure 5-4. Note that 20 dB of rejection is not quite enough to bring the disturbance down below the specification line. Two improvements could be made to this control system in order to increase the disturbance rejection, and bring the ambient vibration down below the specification line. The first would be the addition of a more exotic compensator which boosts the open-loop transfer function gain between 2 and 30 Hz. The problem with employing this filter is that it introduces phase loss

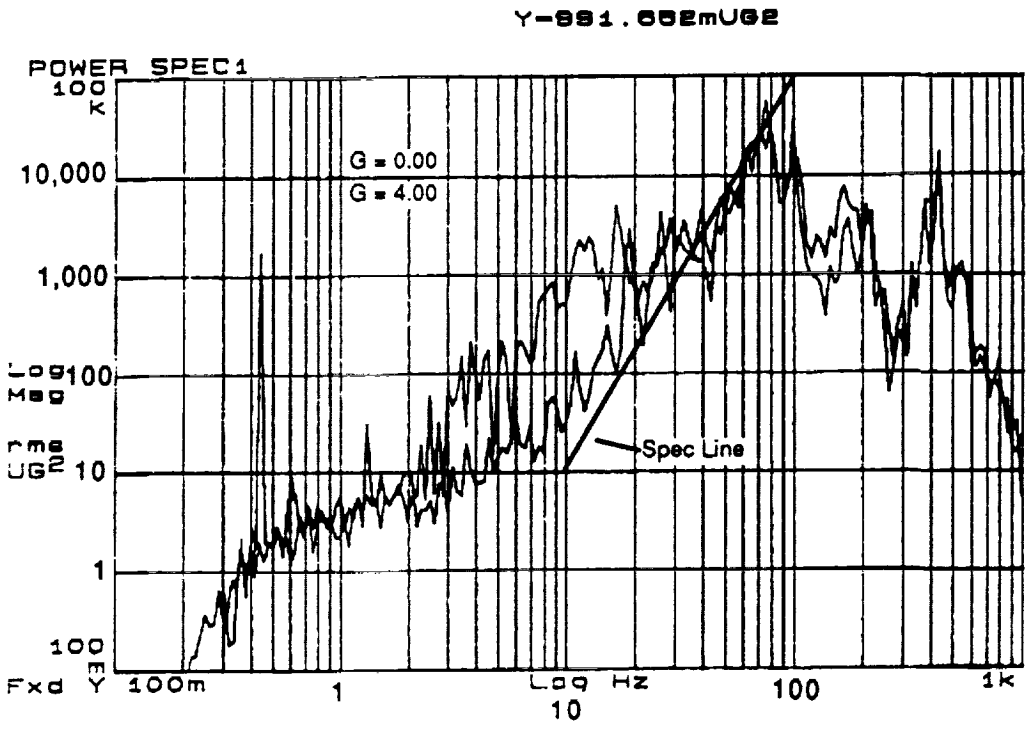

Figure 5-4. Controlled and Uncontrolled PSD Functions Without Injected Disturbance

to the system. The system is already in short supply of phase margin (see Figure 5-2). As was mentioned in Section 5.1, part of the open-loop phase loss may have been due to incorrect electrical hookup of the Sunstrand QA-2000.

The second improvement would be to improve the noise performance of the accelerometer. Figure 3-11 suggests that the noise performance of the Sunstrand QA-2000 accelerometer is adequate for this application. However, possible problems with the electrical hookup of these sensors may be to blame for noise performance which was not consistent with Figure 3-11. The coherence function between two redundant QA-2000 accelerometers, both mounted on the payload was calculated while the loop was active, and while no artificial disturbance was being injected into the system. This function is shown in Figure 5-5. If the noise performance were as presented in Figure 3-11, then the coherence function in Figure 5-5 would have a value very nearly equal to unity, across the frequency band.

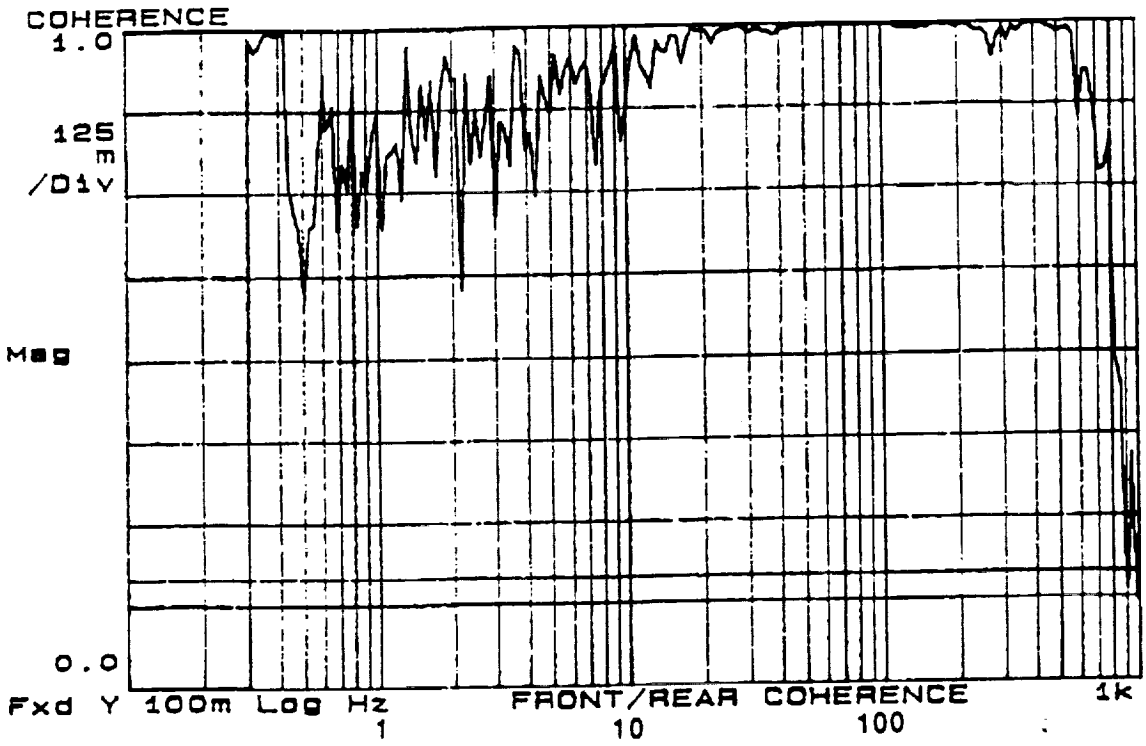

Figure 5-5. Coherence Function Between Redundant Sensors, Mounted on Payload With Control Loop Active and With No Injected Disturbance

Despite the fact that the residual vibration levels were not forced completely below the specification line, the performance data presented in Figures 5-3 and 5-4 does illustrate the feasibility of employing inertial actuators in payload isolation systems. The inertial actuator was not one of the factors which limited the performance of the isolation system.

6.0 THREE-AXIS (3DOF) VIBRATION ISOLATION SYSTEM DEVELOPMENT

6.1 Three-axis (3DOF) Air Bearing Table Configuration

The 3DOF experiment employed a dual-rail air bearing table for the simulation of the orbiter environment, as did the 1DOF experiment. However, the 3DOF air bearing table configuration differs from the 1DOF table in that both rail/skate interfaces are flat. The 3DOF air bearing table configuration is shown in Figure 6-1. When floated, the carriage can rotate about the azimuth axis, as well as translate along both horizontal axes. The rails and skates are considerably wider than those installed on the 1DOF table, so that more weight can be supported. Again, the rails are mounted on a welded steel frame, with leveling adjustments in the feet and in the rail mounts.

One of the lessons learned in the 1DOF experiment was that the structural resonances of the carriage assembly interfere with the control system frequency responses. Resonant spikes often protrude above the 0-dB line in the open-loop transfer function, at frequencies at which there is no phase margin. This effect can cause the control systems to be unstable. The ideal carriage would behave like a pure inertia, exhibiting no resonances whatsoever.

An effort was made to stiffen the 3DOF carriage assembly, so that it would better emulate a pure inertia. Ribs and stiffening struts were added to the 3DOF carriage in order to push the resonances out to higher frequencies. The actuators, sensors and the pneumatic system tubing and fittings were mounted on the carriage, but all other components were located off to the side.

A subtle "dip" in the rails of the 1DOF air bearing table was introduced in order to cage the carriage in some nominal position. This method does not make sense in the 3DOF experiment, so the spring rate of the attachment cables is used as the caging mechanism.

6.2 Three-axis (3DOF) Vibration Isolation Control System

The motion in each of the three axes is controlled by a separate control system. There are thus 3 parallel, classical control systems which are run simultaneously in the 3DOF experiment. The competing approach would be a modern, or "state-space" controller. Such controllers are designed to control multi-input/multi-output (MIMO) systems as a whole, taking into account the coupling effects between the axes of motion. If the designer has modeled the system very

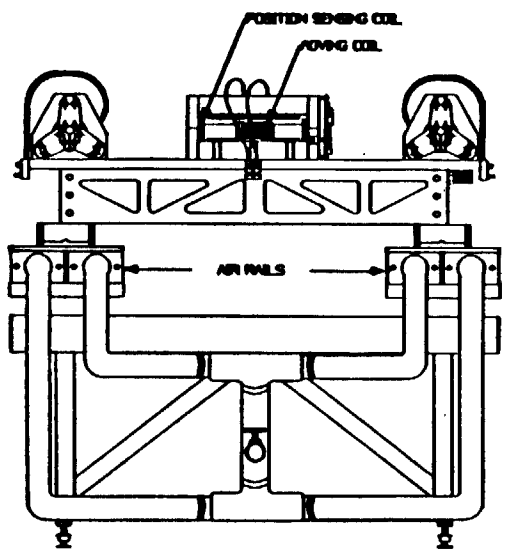

FRONT VIEW

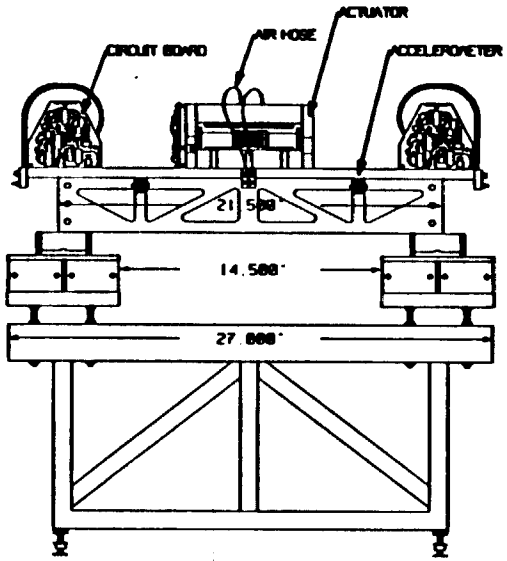

REAR VIEW

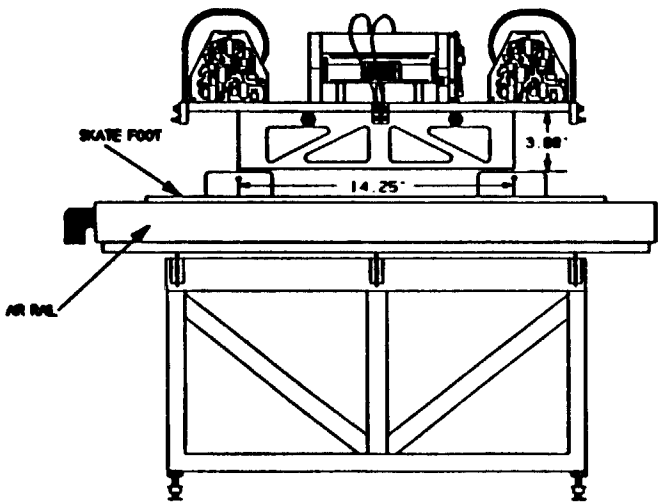

SIDE VIEW

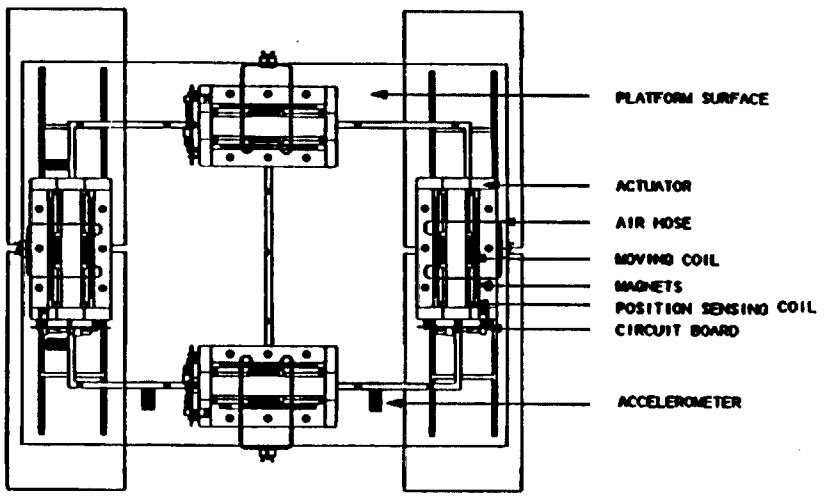

TOP VIEW (carriage only)

Figure 6-1. 3DOF Platform Configuration

accurately, then the coupling between the axes of motion can be removed by a modern controller. The controller which performs this function is essentially the inverse of the plant dynamics matrix, cascaded with a diagonal matrix of easily controllable frequency responses. The resulting system is equivalent to separate, classical control loops, with no coupling between the axes.

Modern control systems have serious shortcomings however. The system under control may have dynamics which change significantly over time. In general a very accurate, time-invariant model of the plant dynamics is *not* available. Unmodeled, poorly placed or time-varying poles can, and generally do, lead to instability. To make matters worse, when a modern control system becomes unstable, or exhibits poor performance, it is not always intuitively obvious what is required to correct the problem. Furthermore, the modern control approach often requires more computer time, because more digital filters must be calculated in a single cycle of the controller. For example, a modern controller for a 3DOF system with second-order dynamics is composed of 6, sixth-order difference equations. Controlling the axes separately (and ignoring the coupling between the axes of motion) requires only 3, third-order difference equations[5] . The question must then be asked: Can the coupling between the axes of motion be ignored?

The only practical way to answer this question is to test the system. If indeed the coupling effects can be ignored, then the compensated, open-loop transfer function indicates the amount of rejection that can be realized by the system. For example Figure 5-2 suggests that rejection of roughly 18 dB should be attainable from the 1DOF system (coupling can undoubtedly be ignored in this system). This rejection is attained at a specific value of the loop gain. If the loop gain is increased, the rejection will improve. However, if the gain is increased above a certain limit, then the system will be unstable. That limit is in general, the phase margin of the control system. Once compensated, these systems are typically tested by increasing the gain until the system becomes unstable. The best rejection is usually realized just at the brink of instability. The loop gain which corresponds to the maximum rejection (near instability) can be predicted from the uncompensated (unity gain) open-loop transfer function. If it is not possible to increase the gain to the predicted value without the system becoming unstable, then there are two possibilities: (1) there is something wrong with the system (i.e. saturated signals, the wrong compensator, malfunctioning components, etc.), or (2) the coupling between the axes of motion cannot be ignored.

[5] Assuming that the same compensation is used for each axis, and that the 1DOF control system described in Section 4.3 is employed

If the coupling between the axes of motion cannot be ignored, then the effort must expended to obtain an accurate model of the system dynamics. A working modern controller can be then be developed and implemented. In some cases it possible to improve the coupling characteristics of the system by altering the physical system itself (mechanically). If the coupling can be reduced to a sufficiently low level, then parallel controllers can be employed after all[6].

Testing of the 3DOF system has shown that 3 parallel, classical control systems are sufficient to control the carriage motion. The coupling effects are less significant than the sensor noise and phase margin limitations.

6.3 Three-axis (3DOF Vibration Isolation System Digital Electronics Hardware and Architecture

The computer configuration for the 3DOF platform was similar to the 1DOF system. Motorola 56001-based Digital Signal Processor (DSP) boards were used to calculate and execute the control algorithms. The A/D converters and D/A converters on the boards were employed because their conversion time was significantly faster than the other VME boards available. This allowed the true performance of the actuator to be investigated without limitations introduced by other hardware in the loop.

Three inputs were required, on for each control loop, and four outputs were needed, one for each actuator. This was accomplished by using two DSP boards, each of which has two input channels and two output channels. The y-axis linear control loop was performed with one DSP and one pair of actuators and the x-axis linear and z-axis' rotational loops were handled by the second DSP and the other pair of actuators. A video tape of the 3DOF platform in operation was recorded and is available for those interested. The sample and update rate was 10KHz for the DSP boards. The high rate preserved phase margin in the control loop allowing the actuator performance to be investigated more accurately.

[6] Blackburn, J. "Methods for Minimizing the Interaction Between Coupled Parallel Control Systems," Fifteenth Biennial Guidance Test Symposium Proceedings, September 1991.

7.0 RESULTS OF 3-AXIS (3DOF) VIBRATION ISOLATION SYSTEM TESTING

7.1 Open-loop Transfer Function Testing

The compensation for each of the three 3DOF control systems was a single, first-order lowpass filter at 5 hertz. After adding stiffening ribs to and removing weight from the carriage (see section 6.1), the structural resonances were moved out to higher frequency. The need for second-order lowpass filters at high frequency was not as dire as was the need in the 1DOF experiment. Furthermore, there were not adequate computer resources to compute additional second-order filters for all 3 of the 3DOF experiment control systems.

Figure 7-1 shows the uncompensated and compensated open-loop transfer functions for the x-axis control system. These Bode plots are measured out to 100 hertz. A similar plot for the 1DOF experiment was presented in Figure 5-1. Comparison of Figures 7-1 and 5-1 verifies that the structural resonances have been moved out to higher frequency.

However, the effects of the structural resonances are still visible at higher frequency. At frequencies below 100 hertz the y and z-axis open-loop transfer functions are quite similar to the x-axis response. Plots of the compensated y and z-axis open-loop transfer functions, measured out to 1000 hertz, are presented in Figures 7-2 and 7-3, respectively. Notice that the structural resonances in these plots are quite pronounced at frequencies above 100 Hz.

7.2 Closed-loop 3DOF Control System Performance Testing

The Endevco 7751-500 linear accelerometers were employed in the 3DOF control systems (see Section 3). These sensors have a noise floor which is too high to realize rejection of the ambient vibration environment. The performance of each of the 3DOF control systems was thus assessed by introducing disturbances with an auxiliary linear, inertial actuator (see Section 5.2). Figures 7-4, 7-5 and 7-6 show the differences between controlled and uncontrolled carriage motion in the x, y and z-axes, respectively. This data was obtained while all 3 loops were closed, at the same time.

The best rejection was obtained in the x-axis, and had a peak value of about 20 dB. This is about as much rejection as can be expected from a active, payload isolation system. The y-axis loop gain does not appear to have been high enough, because the compensated open-loop transfer

function for this axis suggests that over 20 dB of rejection should be attainable. The measured y-axis rejection peaked at about 15 dB. The z-axis performance seems to be limited by the structural resonances at high frequency. No more than about 10 dB of rejection can be realized in this axis before the resonant spikes begin to protrude above the 0-dB line, at frequencies where there is no phase margin.

The rejection performance could be improved by employing sensors which introduce less phase loss to the open-loop transfer function. Another improvement would be to increase the available computer resources so that second-order lowpass filters at high frequency can be added, as they were in the 1DOF experiment.

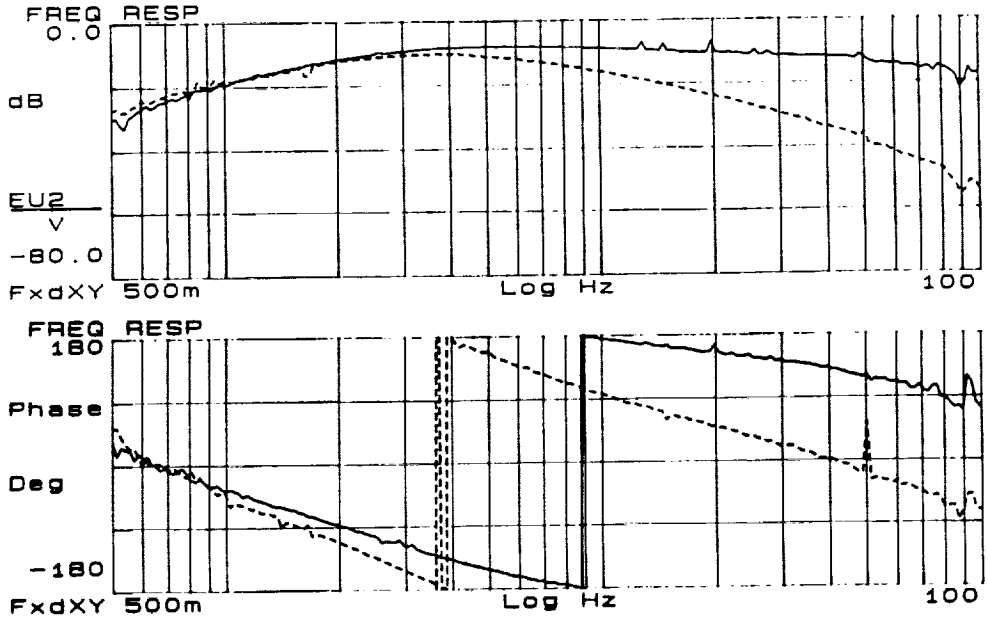

Figure 7-1. Open-Loop Transfer Function of X-Axis Control System, Uncompensated and Compensated

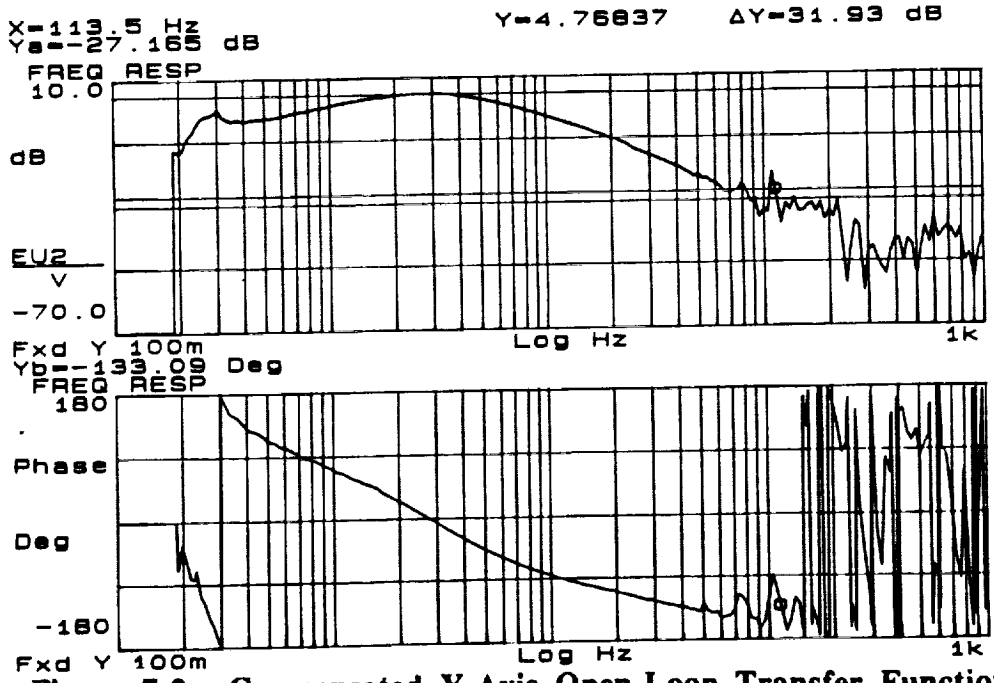

Figure 7-2. Compensated Y-Axis Open-Loop Transfer Function

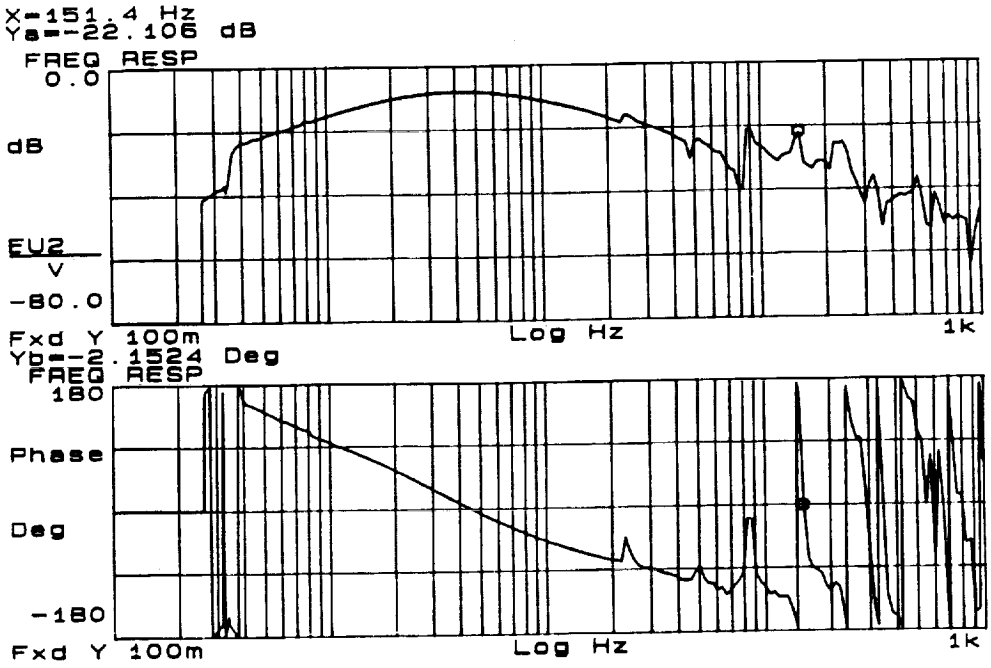

Figure 7-3. Compensated Z-Axis Open-Loop Transfer Function

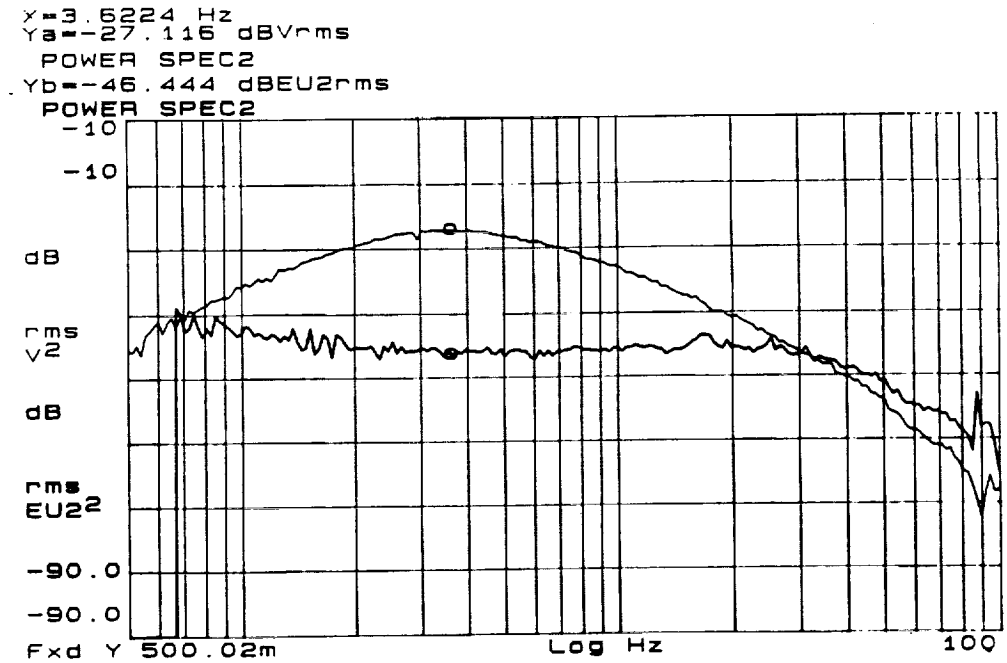

Figure 7-4. psd of X-Axis Carriage Acceleration with Loop Inactive and with Loop Active

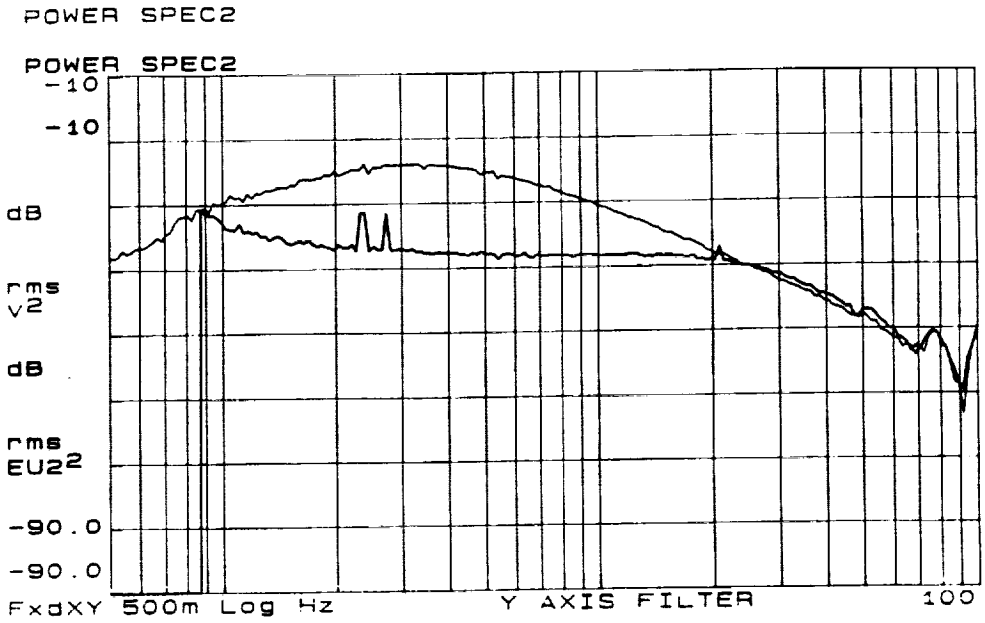

Figure 7-5. psd of Y-Axis Carriage Acceleration with Loop Inactive and with Loop Active

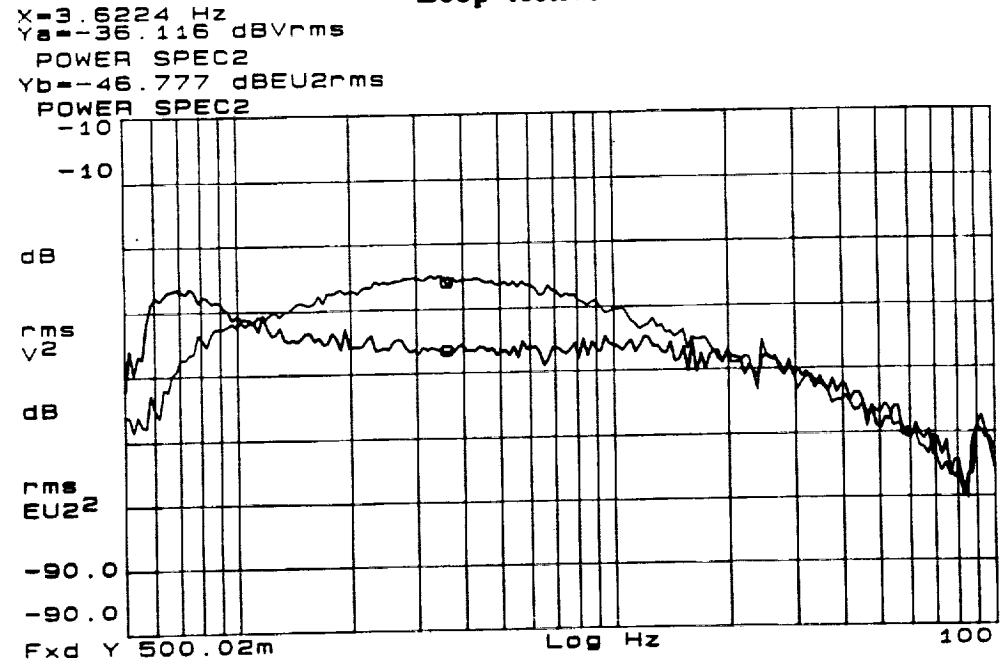

Figure 7-6. psd of Z-Axis Rotational Acceleration with Loop Inactive and with Loop Active

8.0 ADVANCED APPLICATIONS OF THE LINEAR INERTIAL ACTUATOR

8.1 Source Vibration Isolation Systems

A distinction was made in Section 1.1 between payload and source vibration isolation systems. The systems discussed in the previous sections are payload isolation systems. Such systems are intended to reduce the level of vibrations experienced at a payload location. The intent of the 1DOF and 3DOF systems was to minimize the vibration levels experienced on the air bearing carriage.

In contrast, source vibration isolation systems attempt to prevent disturbances generated by the payload from reaching the environment. The disturbances generated by a large piece of rotating machinery can be partially abated before entering the host environment, by placing springs or rubber grommets at the machine/floor interface. This is an example of passive source vibration isolation. Active isolation technology can also be applied to the same problem.

Consider the system in Figure 8-1. A rotating imbalance is created when the mass m, is rotated about point O. The platform P is supported by hydraulic cylinders, and motion is assumed to occur in the vertical direction only. The forces experienced at points (1) and (2) when the system is at rest are due only to the static weight of the system.

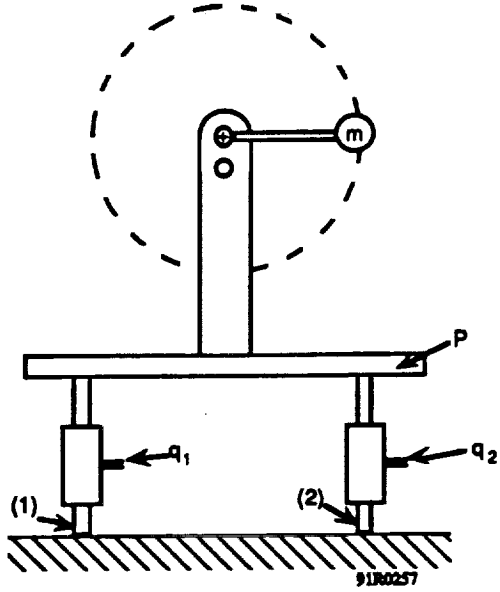

Figure 8-1. Source Vibration Isolation System Employing Relative Force Actuators

Suppose it is desired to hold the forces at points (1) and (2) constant, at their static values, as the mass m, rotates about the point O. Forces can be applied between the platform P, and ground by controlling the flowrates q_1 and q_2, of fluid moving in and out of the cylinders. In order to hold the forces at points (1) and (2) constant, the flowrates must be adjusted so that the platform is free to translate vertically in a given direction, until the rotating imbalance causes the acceleration vector to change direction. The purpose of this example is to illustrate intuitively, that the platform translations which must be permitted in order to accomplish this task are substantial.

Now consider a similar system pictured in Figure 8-2. In this system, the platform P, is supported by a mechanical spring and dashpot. The hydraulic cylinders are replaced by linear inertial actuators which are attached to the platform. The actuators apply inertial forces in the vertical direction. It should be apparent that by transferring the disturbance energy to the actuator proof masses m_p, the vertical position of the platform P, can be held constant, while maintaining constant forces at points (1) and (2).

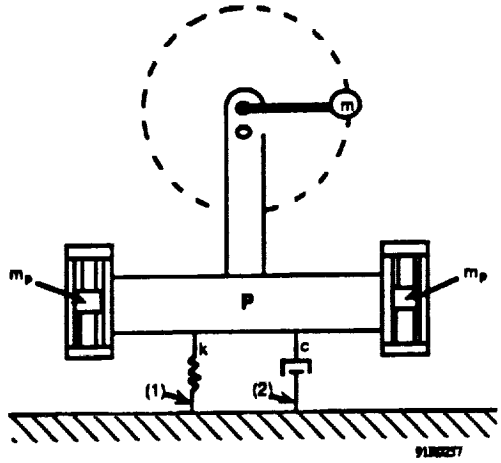

Figure 8-2. Source Vibration Isolation System Employing Linear Inertial Acutators

The two examples presented above illustrate one of the advantages of inertial actuation in source vibration isolation applications. Namely, the "rattlespace" in which the platform P translates (or rotates) can be reduced significantly.

Another interesting application of inertial actuation involves the isolation of an environment from disturbances induced by a person jumping up and down on a trampoline. Suppose that the rotating imbalance m, in Figures 8-1 and 8-2 is replaced by a person jumping up and down on the

platform, P. In order to hold the forces at points (1) and (2) constant, the platform P in Figure 8-1 would have to exert no resistance to the person's step. In this case there would be essentially no firm surface on which to land. The system in Figure 8-2 could be modified for this application without suffering this shortcoming. Indeed, inertial actuation is the *only* way to solve the "trampoline problem".

8.2 Structural Damping

One of the challenges of operating equipment in space is that the structures required to host the equipment have a tendency to oscillate for long periods of time, following a disturbance. There are both passive and active approaches to damping out oscillations in structures. The linear inertial actuator is clearly suited for active damping of this type. The examples below illustrate this point.

Consider the system shown in Figure 8-3. Suppose that the position of the mass m, is changed from position (1) to position (2) by rapidly rotating the hub, and then holding the hub fixed. The mass will overshoot point (2), and begin to oscillate in a cantilever fashion about the point O.

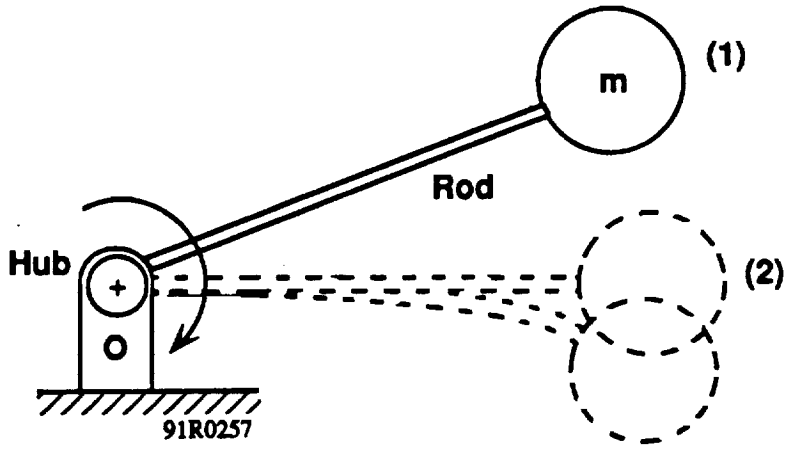

Figure 8-3. Cantilever Oscillation

This oscillation could be counteracted by instrumenting the mass m, with a linear inertial accelerometer and a linear inertial actuator, as shown in Figure 8-4.

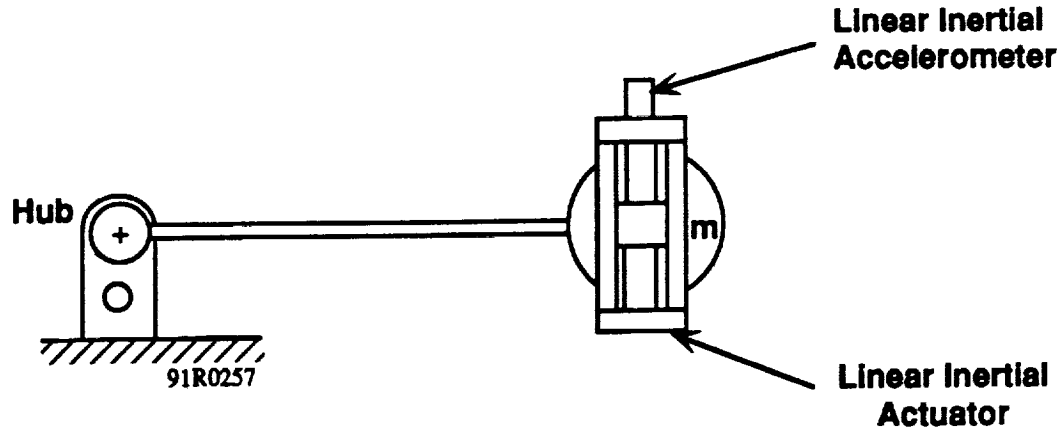

Figure 8-4. Cantelever Instrumented with Linear Inertial Accelerometer and Actuator

The forces applied to the mass by the actuator would be commanded proportionally by the output of the accelerometer. If a relative force actuator were employed to impart forces between the mass m, and ground, then the system would no longer be a cantilever.

Finally, consider the system shown in Figure 8-5. The masses m_1 and m_2 are connected by a flexible rod. The oscillation described by the phantom lines in Figure 8-5 could continue for some time in space, because there is very little damping.

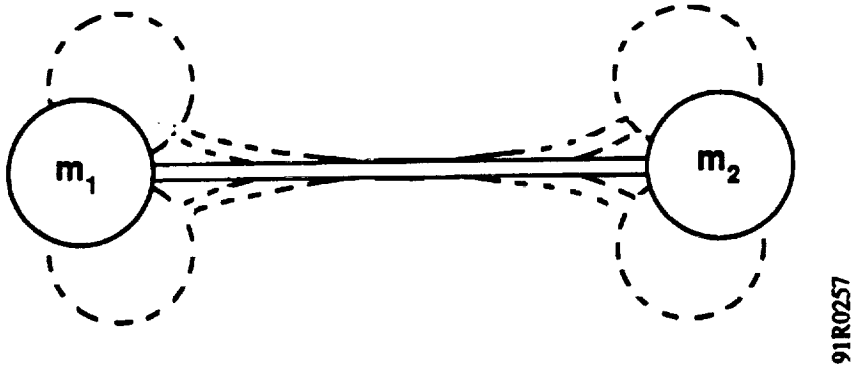

Figure 8-5. Double Cantilever Oscillation

However, both masses could be instrumented with accelerometers and linear inertial actuators as in the last example, making it possible to actively cancel the oscillation. The use of relative force actuators clearly does not make sense in this application.

While they are often far more complicated, oscillations in space and ground-based structures resemble the two simple examples above. These examples demonstrate that the use of momentum interchange is crucial to the control of structures.

9.0 COMMERCIALIZATION PLAN

The intent of the Small Business Innovative Research (SBIR) program is to provide funding for promising technologies in an attempt to create commercial products for small businesses while addressing the sponsor's needs. Phase I of an SBIR is typically a proof of concept effort. Phase II provides funding to develop working prototypes. Phase III is the responsibility of the small business and its focus is to find commercial sponsors or develop the technology into a commercial product.

Efforts to develop the DAMPER inertial actuator were focused in two areas. The first was to protect the intellectual property by perparing and submitting a patent application to cover the device. Working through a patent attorney, ATA reveiwed the possible competitors, prepared the patent application and submitted the documents to the U.S. Patent Office. Approval is expected in 1992.

The second thrust toward commercialization involved promoting the sensor. The main emphasis was placed on displaying the actuator at microgravity conferences and producing a video tape describing the need for and performance principles of the actuator. ATA has had several interested companies and is continuing to investigate actuator applications.

Another possible use for the actuator is to provide force inputs to systems. An inertial modal actuator or a device to inject high frequency vibration into commerical angular rate tables are options being investigated.

The actuator is also being considered for inertial isolation of optical tables by a company with whom ATA has worked previously. To foster development of the actuator, ATA has requested and received permission from NASA Lewis to retain the hardware developed under the Phase II contract. This equipment will be used to support investigations of actuator applications.

10.0 CONCLUSION

Applied Technology Associates, Inc. has developed a linear inertial actuator for space stabilization applications. The actuator was designed and fabricated to meet the requirements of single-axis (1DOF) and three-axis (3DOF) payload vibration isolation experiments. The performance of the actuators was demonstrated by the results of the 1DOF and 3DOF experiments. In these experiments it was shown that linear inertial actuation is equivalent to relative force actuation in payload vibration isolation systems.

The linear inertial actuator has numerous commercial applications including source vibration isolation and structural damping. Indeed, there are a number of applications in which momentum interchange is the only means of actuation that makes sense. The commercialization of the linear inertial actuator is being pursued as the third phase of the SBIR process.

REPORT DOCUMENTATION PAGE

Form Approved
OMB No. 0704-0188

1. AGENCY USE ONLY (*Leave blank*)	2. REPORT DATE	3. REPORT TYPE AND DATES COVERED
	November 1992	Final Contractor Report

4. TITLE AND SUBTITLE

Digital Active Material Processing Platform Effort (Damper), SBIR Phase II

5. FUNDING NUMBERS

WU–694–03–0C

6. AUTHOR(S)

John Blackburn and Dennis Smith

7. PERFORMING ORGANIZATION NAME(S) AND ADDRESS(ES)

Applied Technology Associates
1900 Randolph Road
Albuquerque, NM 87106

8. PERFORMING ORGANIZATION REPORT NUMBER

E–7421

9. SPONSORING/MONITORING AGENCY NAMES(S) AND ADDRESS(ES)

National Aeronautics and Space Administration
Lewis Research Center
Cleveland, Ohio 44135–3191

10. SPONSORING/MONITORING AGENCY REPORT NUMBER

NASA CR–190798

11. SUPPLEMENTARY NOTES

Project Manager, Joseph F. Lubomski, (216) 433–3907.

12a. DISTRIBUTION/AVAILABILITY STATEMENT

Unclassified - Unlimited
Subject Category 31

12b. DISTRIBUTION CODE

13. ABSTRACT (*Maximum 200 words*)

Applied Technology Associates, Inc., (ATA) has demonstrated that inertial actuation can be employed effectively in digital, active vibration isolation systems. Inertial actuation involves the use of momentum exchange to produce corrective forces which act directly on the payload being actively isolated. In a typical active vibration isolation system, accelerometers are used to measure the inertial motion of the payload. The signals from the accelerometers are then used to calculate the corrective forces required to counteract, or "cancel out" the payload motion. Active vibration isolation is common technology, but the use of inertial actuation is such systems is novel, and is the focus of the DAMPER project. In May of 1991 a report was completed which documented the successful demonstration of inertial actuation, employed in the control of vibration in a single axis[1]. In the one-degree-of-freedom (1DOF) experiment a set of air bearing rails was used to suspend the payload, simulating a microgravity environment in a single horizontal axis. Digital Signal Processor (DSP) technology was used to calculate in real time, the control law between the accelerometer signals and the inertial actuators. The data obtained from this experiment verified that as much as 20 dB of rejection could be realized by this type of system. Included in this report is a discussion of recent tests performed by ATA in which vibrations were actively controlled in three axes simultaneously. In the three-degree-of-freedom (3DOF) system, the air bearings were designed in such a way that the payload is free to rotate about the azimuth axis, as well as translate in the two horizontal directions. This is the final report on the DAMPER project. It is a culmination of past (1DOF) and present (3DOF) work, and is intended to provide an overall picture of the project. The actuator developed for the DAMPER project has applications beyond payload isolation, including structural damping and source vibration isolation. This report includes a brief discussion of these applications, as well as a commercialization plan for the actuator.

14. SUBJECT TERMS

Vibration isolation; Microgravity science experiments; Active control; Inertial actuators

15. NUMBER OF PAGES

60

16. PRICE CODE

A04

17. SECURITY CLASSIFICATION OF REPORT	18. SECURITY CLASSIFICATION OF THIS PAGE	19. SECURITY CLASSIFICATION OF ABSTRACT	20. LIMITATION OF ABSTRACT
Unclassified	Unclassified	Unclassified	